

Recent Advances in Ultrathin Chiral Metasurfaces by Twisted Stacking

Zexiang Han, Fei Wang, Juehan Sun, Xiaoli Wang,* and Zhiyong Tang*

Artificial chiral nanostructures have been subjected to extensive research for their unique chiroptical activities. Planarized chiral films of ultrathin thicknesses are in particular demand for easy on-chip integration and improved energy efficiency as polarization-sensitive metadevices. Recently, controlled twisted stacking of two or more layers of nanomaterials, such as 2D van der Waals materials, ultrathin films, or traditional metasurfaces, at an angle has emerged as a general strategy to introduce optical chirality into achiral solid-state systems. This method endows new degrees of freedom, e.g., the interlayer twist angle, to flexibly engineer and tune the chiroptical responses without having to change the material or the design, thus greatly facilitating the development of multifunctional metamaterials. In this review, recent exciting progress in planar chiral metasurfaces are summarized and discussed from the viewpoints of building blocks, fabrication methods, as well as circular dichroism and modulation thereof in twisted stacked nanostructures. The review further highlights the ever-growing portfolio of applications of these chiral metasurfaces, including polarization conversion, information encryption, chiral sensing, and as an engineering platform for hybrid metadevices. Finally, forward-looking prospects are provided.

1. Introduction

A chiral object, by definition, has a nonsuperimposable mirror image of itself. From the spiraling gastropod shells to the left-handed bias of the universe, chirality is of universal significance across both length-scales and disciplines.^[1] Significantly, chirality bears technological implications; for instance, chiral nanomaterials have found many applications in chiral sensing, enantioselective catalysis and polarization-sensitive optics owing to the differential interactions with left circularly polarized (LCP) and right circularly polarized (RCP) light.^[2–5] Therefore, many efforts have been devoted to studying and engineering chiral nanomaterials, with a particular focus on


chiral plasmonic nanoparticles and their self-assembled structures as colloidal suspensions.^[6–9] Recently, beyond noble metal plasmonics, solid-state layered nanomaterials that are rotationally aligned with a defined twist angle are becoming increasingly investigated (Figure 1). Among these are twisted 2D van der Waals (vdW) materials,^[10–12] twisted single-crystal slabs,^[13,14] twisted aligned nanowire thin films,^[15–18] and twisted metasurfaces with periodic subunits^[19–21] (Figure 2). These chiral stacked materials possessing geometric handedness and optical chirality can be seen as truncated and minimalistic versions of supramolecular liquid crystals in the chiral nematic phase or of 3D chiral photonic crystals.^[22–24] Compared to their bulk or multiple-layer counterparts, the fabrication becomes greatly simplified for bilayer or few-layer chiral metamaterials, enabling precise control over the interlayer twist angle to manipulate light-matter interactions. Ultrathin chiral meta-

materials and metasurfaces with tunable optical and chiroptical responses are thus an active field for study.

Twisting achiral layered nanostructures in parallel planes enables engineering of the extrinsic chirality and related optical performance. Specifically, the twist angle from counterclockwise rotation of an upper layer with respect to the beneath one is defined to be positive, $\theta > 0^\circ$, leading to a left-handed stacking geometry.^[10,18] Accordingly, negative twist angle from clockwise rotation gives rise to the right-handed counterpart. Accurate control over the interlayer rotation angle offers flexible manipulation of properties, especially optical activity, of twisted layered systems of a wide variety of monolayer constituents and dimensions. A well-studied system is twisted bilayer graphene (TBG), catalyzing the research on twisted stacked nanostructures over the past few years, especially as many intriguing properties of magic-angle graphene are uncovered.^[28–30] The twist angle dependencies of phonon dispersion,^[31] optical absorption and reflection,^[32,33] circular dichroism (CD) and birefringence,^[10,34] second harmonic generation (SHG),^[35] and photoresponse^[36,37] of TBG have been extensively explored in the past few years. Similar realizations have been reported for twisted nanostructures of other 2D materials such as transition metal dichalcogenides,^[38,39] graphitic carbon nitride,^[40] and hexagonal boron nitride (hBN),^[41] as well as non-2D systems like polymeric thin films or patterned plasmonic nanohole arrays.^[42,43] Therefore, there exists fertile ground for chiral metasurface design

Z. Han, F. Wang, J. Sun, X. Wang, Z. Tang
CAS Key Laboratory of Nanosystem and Hierarchical Fabrication
National Center for Nanoscience and Technology
Beijing 100190, P. R. China
E-mail: wangxl@nanocr.cn; zytang@nanocr.cn

X. Wang, Z. Tang
Center of Materials Science and Optoelectronics Engineering
University of Chinese Academy of Sciences
Beijing 100049, P. R. China

 The ORCID identification number(s) for the author(s) of this article can be found under <https://doi.org/10.1002/adma.202206141>.

DOI: 10.1002/adma.202206141

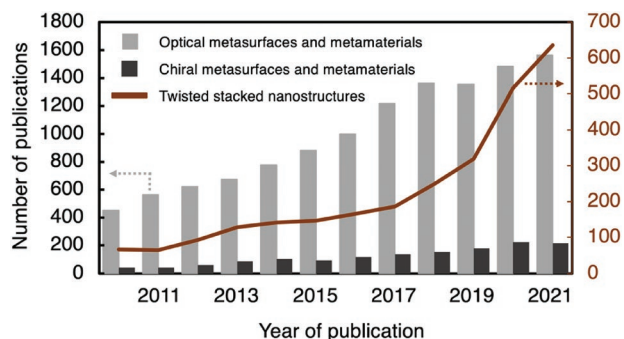


Figure 1. Growing research interests in chiral optical metamaterials and twisted stacked nanostructures. Publication data from Web of Science.

by utilizing different classes of materials, thus enriching both intrinsic materials properties and extrinsic designable device performance. Owing to the structure characteristics at nanoscale (Figure 2), they represent promising ultrathin chiral materials for use as or in highly compact optical devices.^[20]

Herein, we discuss ultrathin chiral nanostructures fabricated by twisted stacking, focusing on their CD responses and relevant applications. Section 2 provides an overview of 2D materials, aligned nanowire thin films, and some traditional metasurfaces that have been used as monolayer constituents.

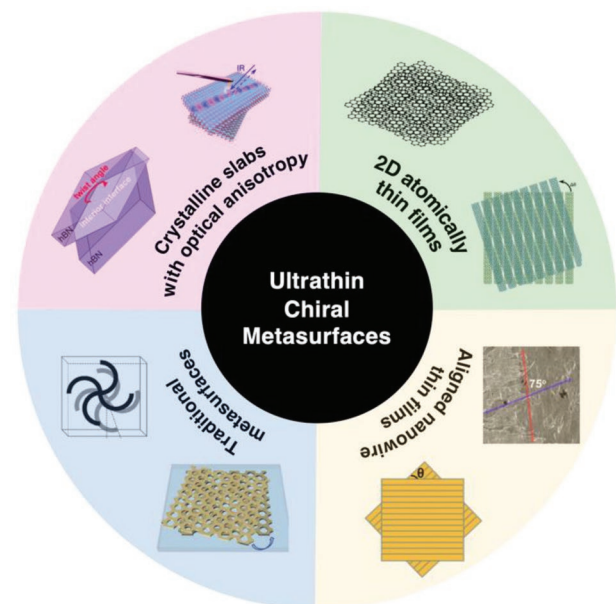


Figure 2. Ultrathin planarized chiral metamaterials in twisted bilayer geometry. 2D atomically thin films: twisted bilayer graphene and twisted bilayer graphene nanoribbon arrays. Reproduced with permission.^[25] Copyright 2020, American Chemical Society. Aligned nanowire thin films: scheme and electron micrograph of a bilayer gold nanowire film. Reproduced with permission.^[15] Copyright 2017, Wiley-VCH. Traditional metasurfaces: twisted bilayer rosettes. Reproduced with permission.^[26] Copyright 2006, American Physical Society. Twisted bilayer plasmonic nanohole array. Reproduced with permission.^[18] Copyright 2017, Wiley-VCH. Anisotropic crystalline slabs: twisted hexagonal boron nitride crystal slabs. Reproduced with permission.^[13] Copyright 2021, American Chemical Society. Twisted bilayer alpha-phase molybdenum trioxide (α -MoO₃) crystals. Reproduced with permission.^[27] Copyright 2020, Springer Nature.

Examples of the fabrication strategies of their twisted stacked structures and the associated practical challenges are introduced. Section 3 briefly recounts the fundamentals of light–chiral matter interactions and the current understanding on the emergence of CD by means of twisted layered stacking of achiral materials. The optical performance of these chiral metasurfaces is quantitatively compared. A multitude of methods used for tuning the CD signals are also critically reviewed. We then discuss in detail the latest studies on the optical and chiroptical applications of twisted double-layer and few-layer metamaterials in Section 4. Finally, we conclude by offering some perspectives on the future research directions of chiral metamaterials. This review is of interest to a broad readership who works in fields such as metamaterials engineering, chiral optics and photonics, and chiral sensing.

2. Materials Systems and Chiral Stacked Structures

2.1. 2D Chiral Thin Films

2D materials possess a large active surface area and low dimensionality, the latter of which is highly desired for use as ultra-compact and lightweight optical/electronic devices. Twistronics that simultaneously leverages twisted stacking and the electronic properties of 2D vdW materials have been envisioned as an emerging electronic technology.^[44] Similarly, one can combine twisted stacking and optical/photonics properties of 2D structures to attain novel twist optics.^[10,11,45] Kim et al. were the first to fabricate cm-scale chiral atomically thin films of graphene.^[10] Monolayer graphene is intrinsically achiral. Through manually twisting two layers of graphene with respect to each other by a specific angle, the resultant bilayers with a thickness of 0.69 nm were imparted a geometric handedness following the direction of rotation (i.e., being clockwise or counterclockwise), subsequently displaying optical chirality. The middle panel of **Figure 3a** exemplifies a left-handed TBG. Apart from semimetallic graphene, other 2D materials with sub-nanometer thicknesses would also be used as monolayers in twisted vdW materials, such as insulating hBN (with bandgap $E_g \sim 5.9$ eV), semiconducting transition metal dichalcogenides ($E_g \sim 1.0$ – 2.5 eV), metallic MXene, magnetic chromium trihalides CrX₃ (X = F, Cl, Br), and high-temperature superconducting oxides, though most chiral stacked structures are not yet experimentally investigated.^[46–48] These 2D materials cover a selective spectral range from the UV to IR,^[49] which is of particular relevance for photodetection,^[50–53] making the chirally stacked structures potential candidates as detectors for circularly polarized light.

Currently, chiral twisted 2D materials are obtained by direct growth via chemical vapor deposition (CVD) or by artificial twisting of monolayers that are either CVD-grown or mechanically exfoliated. Accessing a wide range of twist angles in directly grown twisted 2D materials is fundamentally challenging because the interlayer rotation angle affects the energetics of bilayer or multilayer structure. Taking TBG, e.g., Bernal stacking with a zero twist angle is the most thermodynamically stable, as is the case for graphene layers in natural graphite.^[54] In many CVD-grown bilayer graphene,

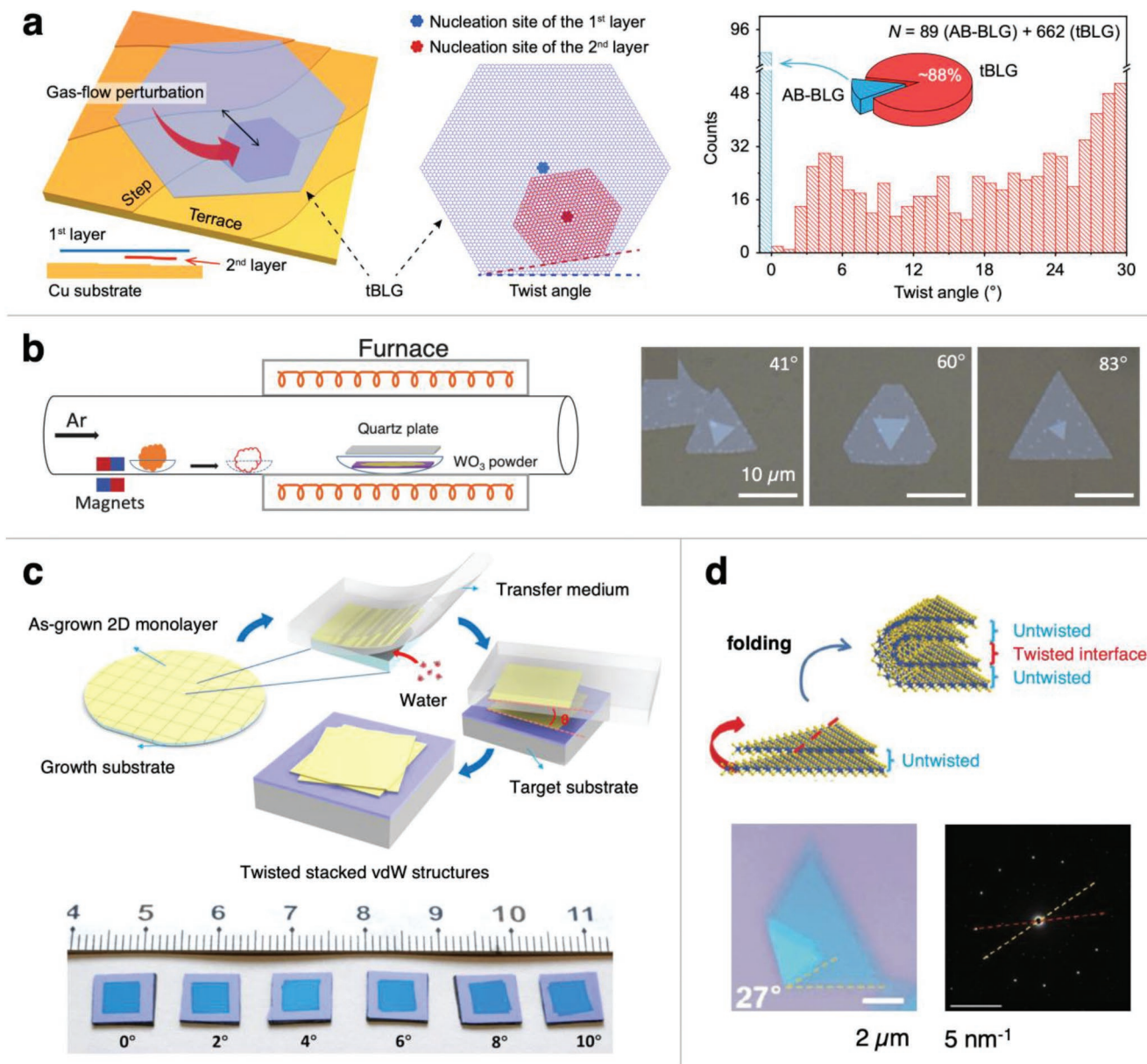


Figure 3. Preparation of chiral stacked 2D vdW materials. a) Direct CVD growth of TBG using a heterosite nucleation strategy and the corresponding twist angle distribution. Reproduced under terms of the CC-BY license.^[58] Copyright 2021, The Authors, published by Springer Nature. b) CVD of twisted WS₂ homobilayers: scheme of CVD setup and optical micrographs of as-grown twisted WS₂. Reproduced with permission.^[60] Copyright 2015, Wiley-VCH. c) Water-assisted transfer for twisted stacking of MoS₂, with photographs of sub-cm²-scale twisted bilayers and trilayers of MoS₂ on a Si/SiO₂ substrate. Adapted under terms of the CC-BY license.^[61] Copyright 2021, The Authors, published by Springer Nature. d) Scheme of folding-induced rotational displacement. Corresponding optical micrograph and selected area electron diffractogram of a 27°-twisted double bilayer MoS₂. Adapted with permission.^[62] Copyright 2022, Wiley-VCH.

a 30°-incommensurate quasi-crystalline structure is also observed, where the 30°-TBG is stabilized by the growth substrate such as Cu(111).^[55] Any other twist angles are energetically unfavorable, thereby making them intrinsically difficult to obtain via growth.^[56,57] To circumvent this, Sun and colleagues proposed a heterosite nucleation strategy by exploiting gas flow perturbation to momentarily drive the system out of equilibrium (Figure 3a).^[58] A large variety of twist angles were accessed using this strategy, with the fraction of twist angles

from 0° to 30° being as high as 88%. Similar attempts were made in the direct CVD growth of twisted double layers of other 2D materials, such as molybdenum disulfide (MoS₂) or tungsten disulfide (WS₂), yet it remains a hurdle to achieve a broad distribution of twist angles (Figure 3b).^[59,60] Additionally, the average lateral sizes of as-prepared 2D vdW domains are relatively small due to the uncontrolled spatial proximity between the nucleation sites. The grown TBG islands have a lateral size of ≈10 μm and that of twisted WS₂ bilayers is even smaller.

These limitations notwithstanding, CVD-grown twisted bilayers are highly desired since there are no interfacial contaminants introduced and a clean chiral interface is maintained, which is paramount to device performance.

Artificial twisting or stacking of monolayers is an alternative means much favored by researchers. Cai and Yu provided an excellent review on the fabrication of TBG by manual assembly of graphene monolayers,^[63] and the strategies discussed within could be extended to prepare any arbitrary chiral 2D vdW structures with a desired layer number by adopting appropriate transfer methods. Here, we highlight a few methods that have been used to construct twisted layered 2D structures with a chiral stacking configuration. First, using a custom-built rotational alignment machine, it is possible to rotate the bottom 2D layer by a designed twist angle followed by transfer of the top monolayer. Such manual twisting allows for customizable twist angles compared to CVD growth, and the precision of the twist angle is determined by the rotational alignment transfer protocol used. For instance, wet transfer of vdW materials in an optical microscope-based alignment transfer machine is able to achieve a twist angle accuracy of less than 1° .^[64,65] Using this method, Lan and colleagues prepared chiral stacked WS_2 bilayers with positive and negative rotation angles, which displayed distinct valley-polarized photoluminescence spectra as well as strong excitonic magneto-chiral anisotropy.^[66] By contrast, direct bonding in a high vacuum guided by reflection high-energy electron diffraction has a higher uncertainty of rotational alignment of $\approx 4^\circ$.^[67] Of note, large-area samples may be prepared through “tear-and-stack” since the maximal lateral size, defined to be the area of the overlapped region, is only limited by the monolayer sample quality and the transfer procedure. Figure 3c exemplifies the twisted layered vdW sample in near cm^2 size. Besides twisting the monolayers after growth, Liu’s group showed the possibility of prerotating the underlying copper CVD growth substrate.^[68] Using a Cu/TBG/Cu sandwich structure, they successfully grew centimeter-sized TBG films with arbitrary twist angles with an angular precision of $<1^\circ$. Second, inspired by origami, researchers attempted to fold 2D materials using an atomic force microscopy or a scanning tunneling microscope to achieve edge-defined rotation angles.^[63,69] Zhang et al. reported a paraffin-assisted folding strategy on nontwisted MoS_2 single-, bi-, or trilayers. This strategy was used to successfully prepare a twisted bilayer, twisted double bilayer, and twisted double trilayer MoS_2 system, respectively, each having only one chiral interface (Figure 3d). For other naturally layered vdW materials, a high-shear exfoliation method could be adopted to fabricate twisted nanosheets in a robust fashion.^[48] Tan et al. prepared twisted V_2C MXene nanosheets with a sub-micron lateral dimension and small twist angles of 2° – 8° by putting nontwisted multilayer MXene samples into a high-shear rotor laboratory mixer.^[48] Although the twist angle control was not discussed in detail in this study, it was said that ensuring a high-shear laminar flow was key to enabling interlayer sliding for small-twist-angle layered MXene. It is reasonably anticipated that oppositely chiral forms of layered MXene would be prepared using this approach by simply reversing the direction of shear flow.

Overall, despite recent progresses, the preparation of high-quality (i.e., large-area and single-crystal) chiral stacked 2D vdW

materials remains a hurdle.^[70] A twisted vdW structure requires single-crystal monolayers for meaningful assignment of twist angles since the angle is based on the rotational misalignment between lattice registries. In realistic samples, pure monocrystallinity is rarely obtained owing to preparation-induced defects, leading to twist angle inhomogeneity and lattice strains.^[70,71] Selected area electron diffraction can only measure the local twist angle confined to the inverse nanometer scale. To validate the homogeneity of twist angles and thus of 2D chiral metasurfaces more globally, two methods capable of mapping the spatial distribution of twist angles at the micron scale have been proposed: i) using a combination of Raman spectroscopic and low-energy electron diffraction imaging,^[72] and ii) employing a nanoscale scanning superconducting quantum interference device, also known as nano-SQUID.^[73] In addition, optical chirality is primarily characterized using commercial CD spectrometers that operate with a beam size that exceeds tens of microns. Obtaining large-area twisted 2D vdW materials for CD measurements and, more importantly, practical applications are thus an ongoing challenge. Last but not least, realizing specific stacking orders requires Angstrom precision in atomic lattice alignment, remaining unfeasible at the current stage. One specific scenario is the stacking-dependent chiroptics of twisted bilayer hBN. Like graphene, hBN adopts a hexagonal lattice structure with two atoms per unit cell. Yet hBN has two different atoms occupying the unit cell, resulting in a broken sublattice symmetry. This feature leads to two families of chiral twisted structures with different atomic registries for bilayer hBN: heteropolar stacking where boron and nitrogen atoms sit on top of each other prior to chiral twisting, and homopolar stacking where atoms of the same polarity are aligned prior to chiral twisting.^[12] Depending on the exact stacking configuration of hBN, its highest CD intensity differs by almost an order of magnitude according to theoretical calculations.^[12] By analogy, it is expected that twisted transition metal dichalcogenides and twisted MXenes will also exhibit stacking-dependent chirality. Much experimental work is needed in this area.

2.2. Directionally Aligned Nanorod-, Nanowire-, or Nanofiber-Based Chiral Thin Films

Thin films of highly oriented nano-objects, such as 1D inorganic nanowires and polymeric nanofibers, can as well be utilized as layered materials to fabricate chiral metasurfaces. Here, nanorods or nanowires instead of single atoms serve as the building blocks. A well-investigated class of this type of chiral twisted nanostructures is chiral photonic crystals with a multilayered configuration, and some natural examples and their engineered counterparts have been reviewed elsewhere.^[74,75] In what follows, only recent examples of ultrathin chiral bilayer or few-layer geometries are discussed.

Langmuir–Schaeffer assembly,^[15,76] grazing incidence spraying,^[17,77] gravity-assisted alignment,^[42] and template-assisted colloidal assembly^[16] have been employed to prepare monolayers in chiral twisted metamaterials. In particular, due to the well-established synthesis protocols for plasmonic nanostructures and plasmon-enhanced light–matter interactions, numerous recent works have investigated chiral plasmonic

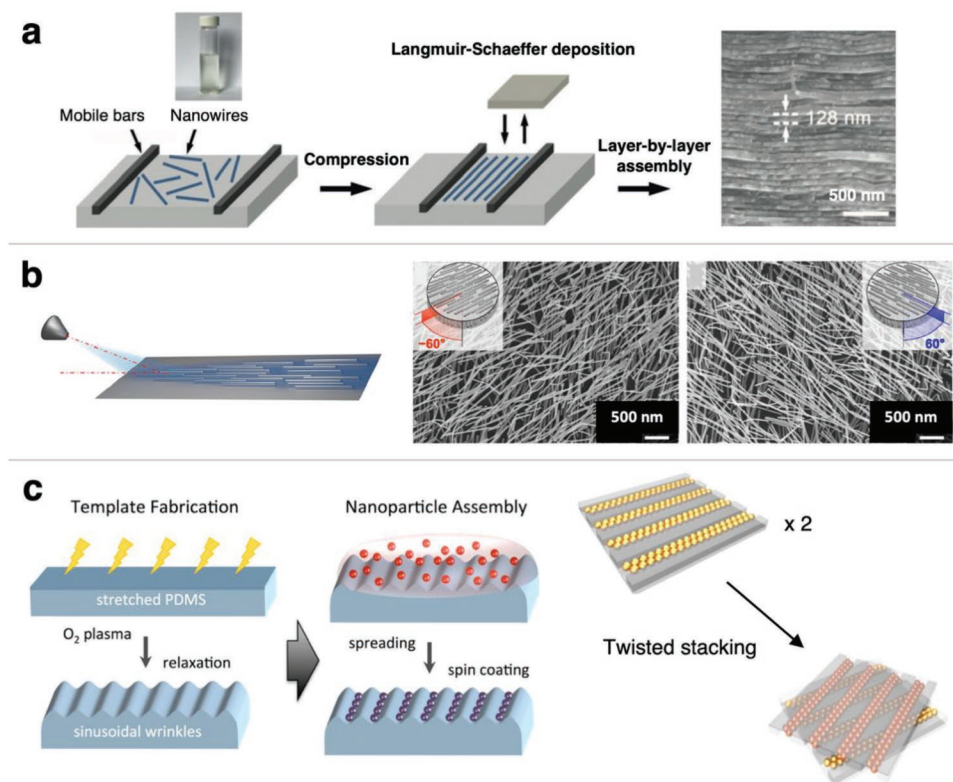


Figure 4. Chiral twisted nanostructures based on aligned nanorods, nanowires, or nanofibers. a) Langmuir–Schaeffer deposition and transfer process for nanowire-based multilayered chiral structures. Adapted with permission.^[76] Copyright 2019, Wiley-VCH. b) Scheme of grazing incidence spraying for aligned nanowires. SEM images showing two enantiomers of AgNW-based chiral bilayer thin films. Reproduced with permission.^[77] Copyright 2021, American Chemical Society. c) Template-assisted self-assembly of nanoparticles using a typical polydimethylsiloxane template. Reproduced with permission.^[81] Copyright 2014, American Chemical Society. Corresponding chirally stacked metasurfaces. Adapted with permission.^[16] Copyright 2021, Springer Nature.

metasurfaces based on orientationally aligned gold or silver nanorods or nanowires.^[15–17,77] By dispersing colloidal inorganic nanowires in a Langmuir trough followed by directional compressing, a highly oriented thin film with a defined monolayer thickness might be obtained (Figure 4a).^[15,76] The same approach enjoys wide applicability to different inorganic nanostructures including ultrathin nanowires of $W_{18}O_{49}$ and $NiMoO_4 \cdot xH_2O$, and even acts as a template to guide the directional assembly of larger-diameter Au nanorods (AuNRs).^[15] Another method for controlling the directional alignment of high-aspect-ratio nano-objects is grazing incidence spraying, also known as glancing angle deposition (Figure 4b). In this approach, dilute suspensions of plasmonic inorganic nanowires or polymeric nanofibrils are sprayed onto a substrate at an off-normal angle, leading to high in-plane anisotropy of as-deposited thin film in centimeter size.^[78] When using Ag nanowires (AgNWs) as the building block, the 2D nematic order parameter S that quantifies the degree of orientation order reached a value of 0.79.^[77] Furthermore, near-unity order parameter, i.e., nearly perfect alignment, was realizable by optimizing the deposition setup and spraying parameters.^[79] Following a layer-by-layer concept, relatively large-area twisted Bouligand nanostructures were prepared. Beyond plasmonic nanostructures, polymeric nanofibers also align into monolayers for chiral

stacking. Gravitational forces were leveraged to align polydiacetylene fibers during topological solid-state polymerization.^[42] The excellent alignment in nanofibrils and microscale fibers was ascertained using atomic force microscopy and polarized optical microscopy, respectively. Lastly, nanowires self-assembled from nanoparticles are alternative candidates. One example was template-assisted colloidal assembly of Au nanoparticles (AuNPs) into 1D chain arrays (Figure 4c). The template, most often being polydimethylsiloxane, was then twisted manually during transfer for chiral stacking. This strategy can be further extended to encompass other monolayer designs, not just 1D arrays, to fabricate chiral metasurfaces with more complex patterns and exceptional chiroptics.^[80]

For directionally aligned nanowire thin films, the monolayer thickness ranges from the nanometer to the micrometer scale, which is tuned by altering the constituent nanorod or nanowire dimensions or alternatively by changing the fabrication parameters (such as the spraying time in glancing angle deposition or the concentration of monomer precursors during drop-casting). The twist angle control over the alignment layers is carried out either during the transfer-assisted assembly or after formation of nanowire arrays, such as in the case of layer-by-layer deposition. Compared to 2D materials, assembling thin films from aligned nanorods or nanowires for chiral metamaterials proves

significantly more forgiving. A nanowire-based thin-film monolayer may be described by a spatially averaged vector pointing in the direction of alignment in the quasi-2D plane. The interlayer twist angle is determined from the macroscopic rotational alignment between the directional vectors of each layer rather than between precise atomic registries. The emergence of chiroptical signals in such chiral stacked bilayers or multilayers does not require perfect alignment between nanowires in a given monolayer. The orientational alignment is quantified using the order parameter given by

$$S = 2 \cos^2 \varphi_i - 1 \quad (1)$$

where the brackets denote the statistical mean and φ_i is the angle between the axis of the i th nano-object and the average orientation vector. Importantly, the calculation of the order parameter can be automated in an image-based analysis such as using the OrientationJ plug-in,^[82,83] and a statistically significant number of optical or electron micrographs are needed. From the materials' point of view, the nanowire or nanofiber building blocks are not necessarily single-crystalline, and a uniform size dispersity of the nano-objects is also not obligatory for chiroptical activities. Lastly, as the materials portfolio for chiral thin films continues to expand, alignment methods that have been used to prepare oriented nanorod- or nanowire-based thin films may also be employed. These include but are not limited to Langmuir–Blodgett assembly,^[84] direct writing,^[85] capillary-assisted alignment,^[86] microfluidic-assisted alignment,^[87] and nanocombing.^[88]

2.3. Chiral Metasurfaces based on Subwavelength Structural Motifs

Metasurfaces containing artificial subwavelength periodic motifs have attracted much attention in the optics and photonics research community for the past two decades.^[89,90] Initially proposed as negative refraction materials,^[91] metasurfaces and metamaterials soon became a versatile toolkit for engineering electromagnetic waves and their propagation and revolutionized the field of transformation optics.^[92] Even though many works have incorporated symmetry-breaking elements to introduce chirality into monolayer metasurfaces, the tunability of their chiral optical performance remains rather limited.^[22,93] Twisted stacking of traditional monolayer metasurfaces thus affords an alternative strategy to introduce extrinsic chirality into the system while offering additional degrees of freedom, such as by the twist angle or interlayer separation distance, in optical control.^[94,95] The idea is the same as that in Sections 2.1 and 2.2: rotationally aligning two metasurface layers at an angle induces configurational handedness, thus imparting or enhancing polarization-sensitive optical properties to the materials. Yet, by contrast with either 2D vdW materials or aligned nanowire thin films, having traditional metasurfaces as the constituent monolayers lends greater control over their optical performance, given the large design parameter space for metamaterials.

Generally speaking, a metasurface is composed of periodically repeated structural subunits, with individual elements

known as the meta-atoms. Changing the shape or configuration of the meta-atom resonators and/or the spacing between adjacent elements alters the coupling between them.^[96,97] For metallic metamaterials, this coupling is effectively described by the plasmon hybridization model.^[98] Numerous designs of the meta-atoms have been put forward (Figure 5). Letter shapes that are either centrosymmetric (such as capital I)^[99,100] or symmetry-breaking (such as capital L or lower-case b)^[94] appear to be a common design theme in fabricating metasurfaces. Other shapes could be as simple as nanocylinders,^[19,20] nanocuboids,^[101] split rings,^[102,103] and crosses,^[104] or as complex as gammadions,^[95,105] rosettes,^[26] and triskelia.^[106] In a bilayer or few-layer geometry, decreasing the interlayer separation distance between meta-atoms increases the interantenna coupling. Translational and rotational displacements between layers are also efficient for actively changing the near-field interactions in an identical metamaterial design.

Using inverted shapes or nanoapertures as the elementary units is another design strategy to pattern metasurfaces, and the nanohole arrays arguably are most well-studied. Wu and Zheng used colloidal lithography, also called nanosphere lithography, followed by transfer-assisted stacking to prepare chiral thin films of periodic Au nanohole arrays.^[18] While this method allows the hole diameter and the lattice periodicity to be changed easily, the 2D hexagonal lattice structure cannot be modified due to face-centered cubic packing of nanospheres, limiting further designability of nanohole arrays. The aperture geometry like circular, triangular, or symmetry-breaking holes is an additional design parameter whose variety only becomes accessible by advanced nanofabrication techniques; for instance, shadow sphere lithography introduces chirality into nanoholes through slanted deposition from various incidences.^[107] Noteworthy, electron beam lithography (EBL) and UV photolithography possess significant versatility in preparing designer metasurfaces. In combination with suitable deposition and lift-off protocols, these two nanofabrication techniques produce high-quality patterns like periodic nanoantennae or nanoapertures with an exceptional spatial resolution.^[108] To fabricate the layered metasurfaces, an overlay EBL approach stands out as a popular choice (Figure 6). Specifically, a dielectric material is used to submerge the bottom metasurface and acts as structural support for the deposition and development of the subsequent layer, and so on.^[19,101,109–111] The interlayer spacer and its thickness is accordingly adjusted to tune the chiral-optical properties of metamaterial. Very recently, Cen et al. fabricated a suspended bilayer chiral metasurface with extraordinary chiroptical performance following single-step EBL exposure.^[112] The top and bottom layers were self-aligned, hence eliminating the need for additional lithographic alignment and planarization processes. Besides EBL, other direct writing lithographic techniques may also be employed, though some limitations exist. For example, focused ion beam lithography suffers from beam damage such as ion implantation that alters the surface properties of metamaterial, whereas laser interference lithography proves inadequate for preparing aperiodic metasurfaces. Additional comparative advantages and disadvantages of common lithographic techniques have been comprehensively reviewed by Su et al.^[113]

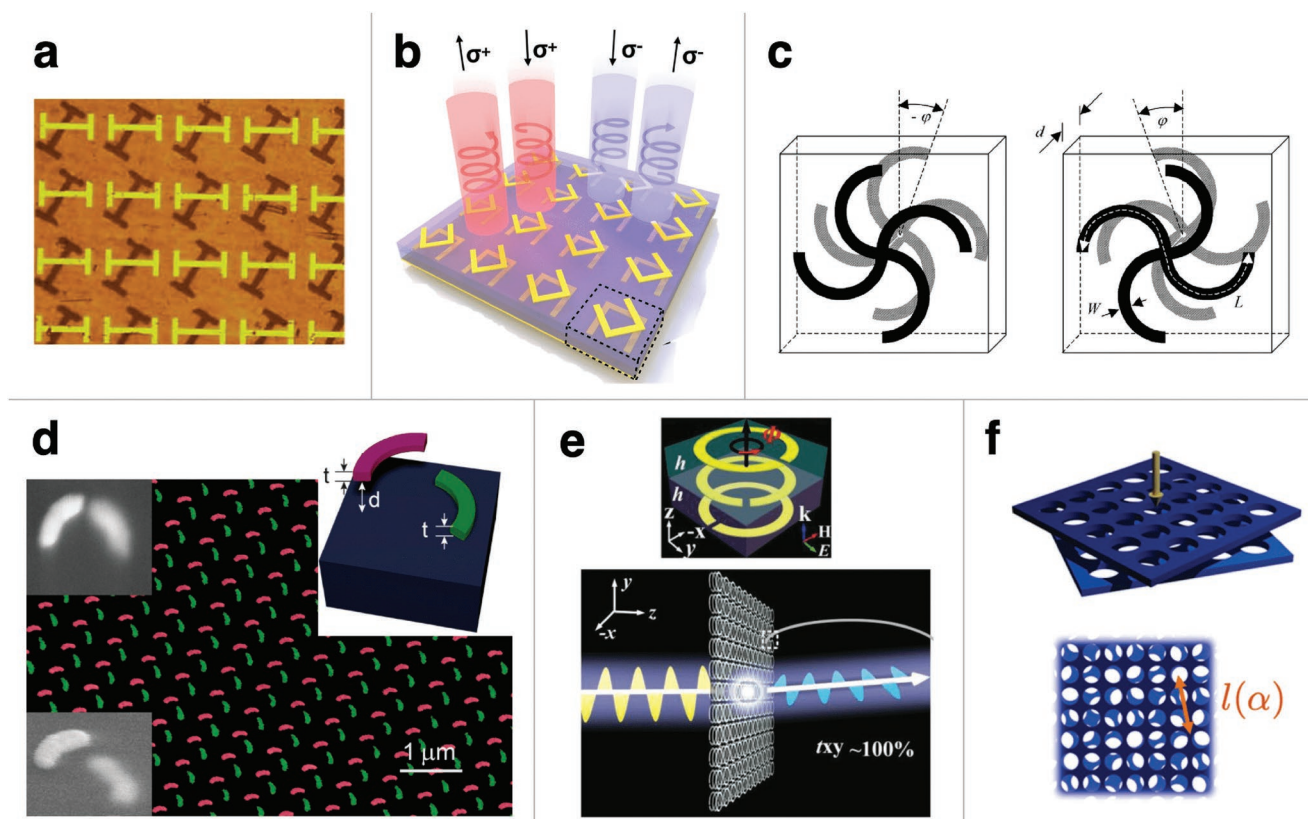


Figure 5. Periodic structural motifs in constituent monolayers for chiral twisted metasurfaces. a) Chiral metamaterials comprising periodically repeating I-shaped units. Reproduced under terms of the CC-BY license.^[99] Copyright 2022, The Authors, published by Optical Society of America. b) Chiral metamaterial based on Π -shaped split ring resonators. Reproduced with permission.^[103] Copyright 2018, American Chemical Society. c) Chiral metamaterial based on twisted rosettes. Reproduced with permission.^[26] Copyright 2006, American Physical Society. d) Chiral metamaterial based on twisted Ag arcs. Reproduced with permission.^[110] Copyright 2014, American Chemical Society. e) Chiral trilayer metasurface of circular split ring resonators as meta-atoms. Reproduced with permission.^[102] Copyright 2019, Wiley-VCH. f) Chiral bilayer photonic crystal slabs and the corresponding Moiré pattern. Reproduced with permission.^[43] Copyright 2022, American Chemical Society.

2.4. Other Miscellaneous Materials Systems

Some other materials systems have been examined to serve as monolayer constituents in planar chiral metamaterials, e.g., biaxial crystalline slabs and unconventional nanopatterned metasurfaces. Recent studies show that monocrystalline slabs with intrinsic in-plane optical anisotropy such as α -MoO₃ or hBN can be stacked in a chiral configuration to elicit or enhance optical chirality.^[13,14,41] Altering the slab thicknesses

during monolayer preparation helps tune the optical performance of chiral stacked structure. The chiral twisting strategy also allows novel optical phenomena, beyond CD, to emerge at the twisted interface. For instance, Lee et al. recently demonstrated how the cathodoluminescence of double multilayer hBN changed continuously with the interlayer twist angle and was further modulated by changing the crystalline slab thicknesses.^[13] In addition, high-precision nanofabrication technique provides unique capabilities to pattern 2D materials or

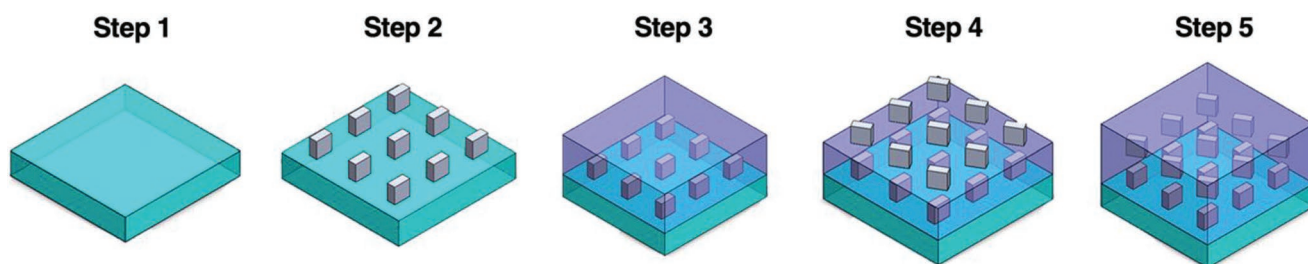


Figure 6. Simplified scheme of overlay EBL for fabricating chiral layered metasurfaces. Step 1: Substrate preparation. Step 2: EBL development of the bottom layer of the metasurface. Step 3: Deposition of the housing medium followed by planarization. Step 4: EBL development of the top layer. Step 5: Second deposition of the same housing medium. Adapted with permission.^[101] Copyright 2020, American Chemical Society.

thin films into desired geometries for complex monolayer designs. One example is graphene nanoribbon (GNR) array that could be prepared from a precursory sheet of single-crystal monolayer graphene via EBL patterning. Numerical simulation showed that twisted bilayer GNR arrays would produce a giant CD response^[114] and act as a hyperbolic Moiré metasurface capable of photonic dispersion engineering.^[25] Nevertheless, similar to many chiral 2D thin films, the experimental realization of twisted bilayer GNR arrays remains challenging.

3. Induced Circular Dichroism of Chiral Twisted Metasurfaces

3.1. Basics of Light–Chiral Matter Interactions

In a chiral metamaterial that is considered a continuous bi-isotropic chiroptical medium, there is coupling between the electric and magnetic fields of the incident light wave.^[26] The constitutive relations that describe the light–chiral matter interactions are given by^[2]

$$\begin{bmatrix} \bar{D} \\ \bar{B} \end{bmatrix} = \begin{bmatrix} \epsilon & \chi + i\kappa \\ \chi - i\kappa & \mu \end{bmatrix} \begin{bmatrix} \bar{E} \\ \bar{H} \end{bmatrix} \quad (2)$$

where \bar{D} = electric displacement field, \bar{B} = magnetic induction field, $\epsilon = \epsilon_0 \epsilon_r$ = permittivity of material, $\mu = \mu_0 \mu_r$ = permeability, χ = the dimensionless magneto-electric parameter, and $\kappa = \kappa' + i\kappa''$ = dimensionless complex chirality index quantifying the cross-coupling between the electric field \bar{E} and magnetic field \bar{H} passing through the medium. Since \bar{D} and \bar{E} are parity-odd whereas \bar{B} and \bar{H} are parity-even, the chirality index κ relating these two physical quantities is also parity-odd, thereby contributing to optical chirality.^[115] Also pertinent to this are the refractive indices of the chiral medium for RCP and LCP light, given by

$$n_{\pm} = \sqrt{|\mu_r \epsilon_r|} \pm \kappa \quad (3)$$

It is noted that materials properties like permittivity should be represented by tensors rather than a constant or scalar to fully parameterize the anisotropy of material. In the parameter space, most materials can be broadly categorized per their values of permittivity and permeability being positive or negative, and some traditional metamaterials have been engineered to realize unnatural optical activities where ϵ and μ are simultaneously negative.^[116] The permittivity and permeability of most materials are well-documented in the literatures, and their frequency- or wavelength-dependencies are generally described by considering a classical damped oscillation model. As for the artificial subwavelength metamaterials, effective medium descriptors can be either experimentally measured or numerically simulated.^[104,117,118] In particular, the Ω -particle model has been employed to explain the electromagnetic resonances in twisted bilayer crosses or gammadians.^[119,120] Corresponding expressions for the effective chirality indices κ are also analytically derived using this model. The transmission-line theory applies especially well to metasurfaces based on plasmonic nanoantennae.^[121,122] The electromagnetic waves at

the dielectric-chiral medium interface for a chiral slab of finite thickness were studied by Bassiri et al.^[123] A similar treatment for atomically thin chiral double-layers and their far-field chiral optics was provided by Zhang et al., detailing the interplay between electric, magnetic, and chiral surface conductivities.^[11]

In this review, we are mainly interested in the emergence of CD response in a chiral stacked structure at normal incidence, which arises from the differential absorption or attenuation of RCP and LCP light passing through it. Therefore, by definition, optical CD is given by

$$CD = \Delta A = A_- - A_+ \quad (4)$$

where A_{\pm} represents the absorbance of RCP and LCP light, respectively, and CD takes on dimensionless values from -1 to $+1$ in this regard. The difference in absorption of LCP or RCP light is characterized by a difference in the amplitude of the transmitted electromagnetic waves, which gives rise to a polarization ellipse illustrating the relative phase between the two orthogonal polarization components of the electric field. This polarization ellipse evolves through the chiral medium in the direction of light propagation, and upon exiting the chiral medium, the transmitted light wave becomes elliptically polarized, defined by an ellipticity angle Ψ in units of degrees ($^{\circ}$). Readers are referred to an excellent review by Collins et al. for a clear visualization of this polarization ellipse and a more elaborate discussion on this topic.^[2] This ellipticity parameter is typically measured by laboratory CD spectrometers in an indirect fashion and is given by^[2,120]

$$\Psi = \arctan \left(\frac{\sqrt{I_+} - \sqrt{I_-}}{\sqrt{I_+} + \sqrt{I_-}} \right) \quad (5)$$

where I_{\pm} is the intensity of the transmitted RCP or LCP light, respectively, although there exist other expressions or definitions of the ellipticity angle.^[2,16,19,20] Often times, when converted to radians, $\Psi \ll 1$, it can be shown that, under small-angle approximation

$$\Psi \approx k_0 d \kappa'' \quad (6)$$

where k_0 = magnitude of the wavevector and d = thickness of the chiral thin film.^[120] It should be noted that CD and ellipticity are distinct concepts; nevertheless, the field has favored the term “circular dichroism” to encompass both meanings, leading to both dimensionless CD values that are true CD as well as CD values in units of degrees that are in reality ellipticity angles. For convenience and to attract a broader audience, we will concede and refer to both as CD where appropriate. CD or ellipticity in a chiral metasurface can be calculated numerically such as using ab initio density functional theory,^[10] finite element method,^[101,124] finite-difference time domain method,^[16,18,125,126] and transfer matrix method (including Mueller matrices).^[14,15,77] When light with a linear polarization passes through the chiral metasurface, the induced chiroptical response is quantified by the optical rotatory dispersion (ORD), which relates to CD through the Kramers–Kronig relation.

Another intrinsic property key to describing the interaction of electromagnetic waves with a subwavelength chiral

metamaterial is the superchiral field, also termed “optical chirality.”^[127] The superchiral field that measures the local chiral density of an electromagnetic field becomes enhanced and concentrated in close proximity to the chiral nanostructure compared to the original incident LCP or RCP light. The optical chirality is mathematically defined as^[2,115]

$$C = \frac{\epsilon}{2} \bar{E} \cdot (\bar{\nabla} \times \bar{E}) + \frac{1}{2\mu} \bar{H} \cdot (\bar{\nabla} \times \bar{H}) = -\frac{\omega \epsilon_0}{2} \text{Im}[\bar{E}^* \cdot \bar{H}] \quad (7)$$

where the asterisk denotes the complex conjugate of a field. Such superchiral fields have been theoretically investigated and experimentally observed in a number of disparate materials systems including plasmon cavities, all-dielectric metasurfaces, and nanohole arrays.^[16,18,107,128–131]

3.2. Emergence of CD from Twisted Stacking of Achiral Monolayers

The requirement for the emergence of optical chirality lies in the chirality index κ . Indeed, Section 3.1 highlights how CD measured as an ellipticity angle directly relates to the imaginary part of κ . Stacking monolayer materials in a twisted fashion introduces geometrical or structural handedness, whereby in a bilayer configuration rotating the top layer counterclockwise would produce a left-handed enantiomer, and right-handed if clockwise. The two enantiomers, linked by mirror symmetry, would then possess different chirality indices κ such that opposite chiroptical responses like CD signals are observed. This is similarly seen in colloidal suspensions of mutually twisted AuNR dimers behaving as chiral meta-molecules.^[132] Phenomenologically speaking, the optical chirality originates from the presence of a chiral twisted interface. This could explain i) why twisted bilayers with opposite rotation angles produce opposite CD responses, and ii) why a twisted trilayer nanostructure where the two interlayer twist angles are equal in magnitude but opposite in sign generates a net zero CD.^[10]

Section 2 illustrates a library of originally achiral materials systems that have been used to fabricate chiral twisted bilayer or few-layer nanostructures: including 2D vdW materials, aligned nanowire thin films, and dielectric or plasmonic metasurfaces. While the existence of CD signals across different materials systems may be justified using the geometrical chirality argument, the observed CD responses in terms of magnitude, peak position, and bandwidth need to be rationalized on case-by-case basis. For example, the optical chirality in both TBG and hBN is explained by the surface-current-induced in-plane magnetic moment that is associated with the interlayer optical transitions (Figure 7).^[10,12,45,133] In particular, the CD peak position of TBG aligns well with the energy interval of the newly emerged van Hove singularities in the hybridized density of states due to interlayer coupling.^[10,33,134] Importantly, these energies are away in position from the main absorption peak at 270 nm owing to π -orbital electronic transitions in monolayer graphene or graphite materials, highlighting the fact that the origin of CD peaks in chiral 2D systems deserves a close and tailored examination such as by looking at the corresponding electronic density of states of the twisted layer.^[12] The spectral

engineering of chiral response of twisted plasmonic metamaterials, on the other hand, is relatively straightforward. In the case of the twisted bilayer Au nanohole arrays by Wu and Zheng,^[18] the CD peak position was aligned with the spectral position of the transmission valley that was characteristic of surface plasmon polariton resonance mode.^[18,135]

Table 1 summarizes the CD responses of some chiral metamaterials in a bilayer geometry reported in the literature, without incorporating any interlayer medium. This table is roughly arranged in the order of increasing spectral wavelength where either broadband or multiband CD response is observed. Notably, the obtained CD signals/peaks are seen in a wide range of electromagnetic spectral regions from UV to visible and mid-IR. So far, the majority of research efforts have been devoted to engineering functional chiral nanostructures with CD in the visible regime,^[8,76] which are also easily accessed by chiral bilayer metasurfaces. Most biomolecules such as amino acids or proteins only display weak chiroptical signals in the UV. Using calculations, Ochoa and Asenjo-Garcia demonstrated that twisted bilayer hBN present CD signals in the UV region (Figure 7e).^[12] As for the IR regime, chiral materials exhibiting enhanced CD in the mid-IR, which has implications for bioimaging, remain scarce.^[136–138] Numerical simulation indicated that both twisted bilayers of 1D arrays of GNRs as well as those of α -MoO₃ slabs could be engineered to produce giant mid-IR CD signals.^[14,114] Overall, the CD of chiral metasurfaces reported in the literatures could be as high as $>10^\circ$ or as low as a few mdeg, spanning over nearly four orders of magnitudes (Figure 8).

Besides CD, both the g -factor and thickness-normalized ellipticity are common metrics to quantify the optical performance of planarized chiral nanostructures. The dimensionless g -factor or dissymmetry factor measures the chiroptical anisotropy of a material at a given wavelength and is defined as^[17,77]

$$g = \frac{\Delta A}{A} = \frac{A_- - A_+}{\frac{1}{2}(A_- + A_+)} = \frac{\Psi \text{ in mdeg}}{32982 A} \quad (8)$$

The g -factor of a material is its CD normalized to the absorbance under linearly polarized light as illustrated by Equation (8). For reference, chiral amino acids or proteins have a g -factor that usually falls within the range from 10^{-4} to 10^{-3} . Some engineered chiral plasmonic nanostructures either as layer-by-layer assemblies or as cellulose-templated nanocomposites achieve much a higher g -factor value of 0.1–0.2, albeit still far from the absolute maximal g -factor of 2.^[140–142] Ultrathin chiral metasurfaces with many degrees of design freedom can be built to display exceptionally high g -factor. Probst et al. investigated the chiroptics of plasmonic metasurfaces based on self-assembled AuNP chain arrays and found that the g -factor reached 0.71 at 1250 nm.^[16] Even more impressively, Wu et al. used spray-induced aligned AgNWs to fabricate 45°-twisted bilayers with a polyelectrolyte interlayer, and the resultant thin film obtained a maximum g -factor of 1.6 in the near-infrared when the interlayer thickness was meticulously tuned to 200 nm.^[17] Thickness-normalized ellipticity in units of $\text{deg } \mu\text{m}^{-1}$ is particularly useful for characterizing chiral thin films. This is because CD magnitude can be engineered by simply increasing the thickness of the metasurface for enhanced absorbance; by normalizing against

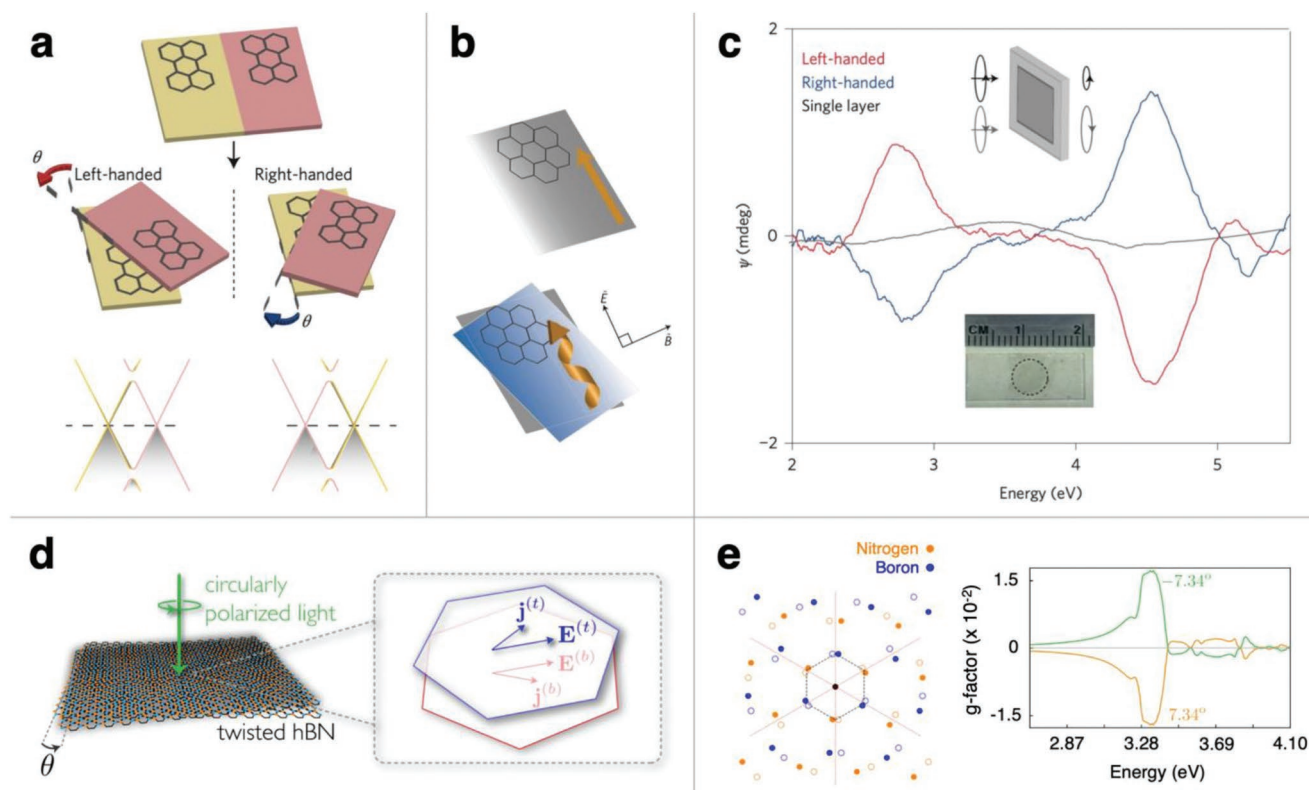


Figure 7. Origin of CD response in chiral twisted 2D bilayers. a) Chiral stacking in twisted bilayer graphene and the corresponding hybridized Dirac cones showing the interlayer optical transitions with opposite polarities. b) Scheme illustrating the generation of a dynamic surface current in achiral and chiral materials when light excites an electric dipole. In the chiral medium, current counterflows adopt a solenoid-like shape in response to the polarization of the incident field. This then engenders an in-plane magnetic dipole moment. c) CD spectra of chiral stacked bilayer graphene and achiral monolayer graphene. Reproduced with permission.^[10] Copyright 2016, Springer Nature. d) Twisted bilayer hBN and generation of surface currents. Adapted with permission.^[12] Copyright 2020, American Physical Society.

its thickness, we arrive at a more design-specific metric useful for performance optimization. Figure 8 summarizes thickness-normalized ellipticity along with the absolute magnitude of ellipticity signals achieved in some chiral twisted metasurfaces. Depending on the monolayer materials and metasurface design, the thickness-normalized ellipticity ranges from $0.8 \text{ deg } \mu\text{m}^{-1}$ for aligned $\text{W}_{18}\text{O}_{19}$ nanowire-based thin films to $109 \text{ deg } \mu\text{m}^{-1}$ for twisted AuNR metasurfaces, spanning over two orders of magnitude. For reference, organic thin films of mono- or disaccharides have thickness-normalized ellipticity of only $\approx 10^{-2}$ in the deep UV.^[143] In particular, we note that chiral stacking traditional metasurfaces with periodic inclusions while embedding them in a dielectric medium can obtain ultrahigh values of both the CD magnitude and the thickness-normalized ellipticity. Exceptionally, an extremely high thickness-normalized ellipticity of $\approx 1000 \text{ deg } \mu\text{m}^{-1}$ was recorded in a chiral organic monolayer thin film of prolinol-derived squaraine, accompanied by a thickness-independent g -factor of 0.75.^[144] Considering antenna-based designer metasurfaces, recent studies have demonstrated the possibility of realizing near-perfect CD response mediated by bound states in the continuum, whereby at a given resonant wavelength the absorption of light of a specific polarization state is maximized.^[145,146] Lessons learned on tailoring chiral resonance coupling could well be applied to twisted stacked

metasurfaces.^[147] As the research on ultrathin chiral metasurfaces is at its inchoate stage, there is still much room for improvement, either experimentally or theoretically, in maximizing performance metrics such as CD, thickness-normalized ellipticity, and the dissymmetry factor.

The chiral stacked metasurfaces are highly attractive for optical investigations. Twisted stacking of achiral (or even intrinsically chiral) monolayers could open doors for a myriad of chiroptical applications that target specific wavelengths of operation. Of note, a machine learning framework has been successfully developed to design chiral twisted metasurfaces with ultrahigh CD response at a predefined wavelength.^[103] Using 2D vdW materials or subwavelength metasurfaces as the monolayers further enables the engineering of exotic optical phenomena not found in bulk counterparts.^[92,148] The materials systems listed in Table 1 merely constitute a fraction of all known materials and employ very simple designs. For example, the CD response of a twisted bilayer metasurface likely depends on the building blocks in the monolayer, such as the diameter and length of nanowires or the size of plasmonic nanoparticles used in templated metasurface. Therefore, there exist endless possibilities to engineer the optical chirality of ultrathin chiral metamaterials from both materials selection and design points of view.

Table 1. Examples of twisted homobilayer structures and their CD responses.

Constituent monolayer materials and references	Bilayer thicknesses	Operational wavelengths investigated	Highest CD or ellipticity (corresponding spectral position)
Graphene ^[10]	<1 nm	250–620 nm	±4.3 mdeg (340 nm)
hBN ^[12]	<1 nm	300–460 nm	±0.17% (375 nm)
Polydiacetylene film ^[42]	300 nm	300–700 nm	±10.6° (660 nm)
Aligned AuNW-based thin film ^[15]	180 nm	300–900 nm	±2.0° (900 nm)
Au nanoholes array ^[18,139]	70 nm	600–1000 nm	±530 mdeg (700 nm)
AuNP dimer chain array ^[16]	200 nm	500–1500 nm	±11.3° (1240 nm)
Aligned AgNW-based thin film ^[17]	100 nm	250–2000 nm	±3.7° (380 nm)
Graphene nanoribbon array ^[14]	<1 nm	12–16 μm	±4.9° (13.8 μm)
α-MoO ₃ crystal slab ^[14]	3300 nm	10–22 μm	±89% (14.4 μm)

3.3. Tunability of CD Signals in Chiral Twisted Metasurfaces

Besides changing the monolayer material or metamaterial design, various means have been developed to tune the CD response in terms of their sign, magnitude, spectral position, and spectral shape. These are summarized in **Figure 9** and discussed in detail below.

A key degree of freedom in engineering chiroptical responses of flat metasurfaces is the interlayer twist angle, which may be precisely controlled thanks to advances in materials synthesis and nanofabrication. An untwisted double-layer metasurface is achiral, displaying zero CD across the entire electromagnetic spectrum, provided that there are no symmetry-breaking elements in the monolayers. When such a bilayer becomes twisted, the structural chirality is transferred into optical chirality with the same handedness, where the sign of the CD signal is reversed when reversing the twisting direction (**Figure 9a**). Rotational periodicity is another key factor in determining the twist-angle-dependency of chiroptical properties. If the constituent monolayer has an n -fold symmetry, the CD or g -factor of twisted bilayer structure experiences a rotational periodicity of $360^\circ/n$. For chiral bilayer thin films based on aligned nanowires or nanorod dimers whose building blocks have a twofold symmetry, the untwisted (0° or 180°) bilayer and the 90° -twisted bilayer display zero CD. As a result, the CD extremum is expected to occur when the interlayer twist angle is at $\pm 45^\circ$, as corroborated by a few examples.^[15,16,19] For others, the rotational periodicity is only applicable to the spectral shape or peak position rather than the magnitude of CD achieved.^[18] **Figure 9a** shows the twist-angle-dependency of CD in chiral 2D bilayers of graphene, with the CD signals originating from the interlayer optical transitions in TBG. A rotational periodicity

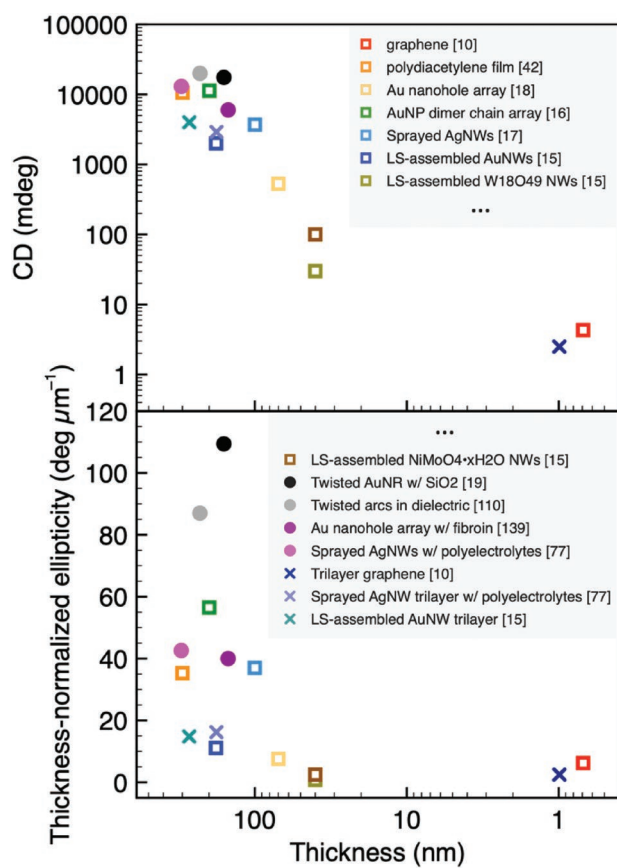


Figure 8. Comparison of CD responses of ultrathin chiral metamaterials in a twisted bilayer or trilayer geometry. Chiral bilayers with no interlayer media are in open squares, chiral bilayers with dielectric interlayers are in closed circles, and chiral trilayer systems are represented by crosses. Only data from the best-performing designs are included.

of 60° in TBG with a sixfold symmetry is ascertained.^[10] For specific metasurface designs, the interlayer twist angle enables spectral wavelength tuning of the CD signal, as seen in nanohole arrays.^[18]

Another strategy to tune the CD signal in chiral twisted metasurfaces is by changing the number of monolayers. In one aspect, increasing the layer number results in enhanced absorbance and therefore CD intensity. This is logically similar to the concentration-dependency of CD response for solutions of amino acids^[149] or colloidal suspensions of plasmonic nanoparticles. Nevertheless, modifications to the CD spectral shape do not follow a definite trend when increasing the layer number while keeping the twist angle unchanged. For twisted rosettes, the spectral shape undergoes numerous changes;^[150] whereas for twisted aligned Au nanowire thin films, the broadband CD signal is retained across the visible-near IR region investigated, and the maximal CD is enhanced but soon saturates upon further increasing the layer number (**Figure 9b**).^[15] Moreover, when using a tri- or multilayer stacking configuration, changing two or multiple twist angles allows us to program CD spectra with increased complexity.^[10]

It has been recognized in some material systems that the characteristics of the first or top layer in direct contact with

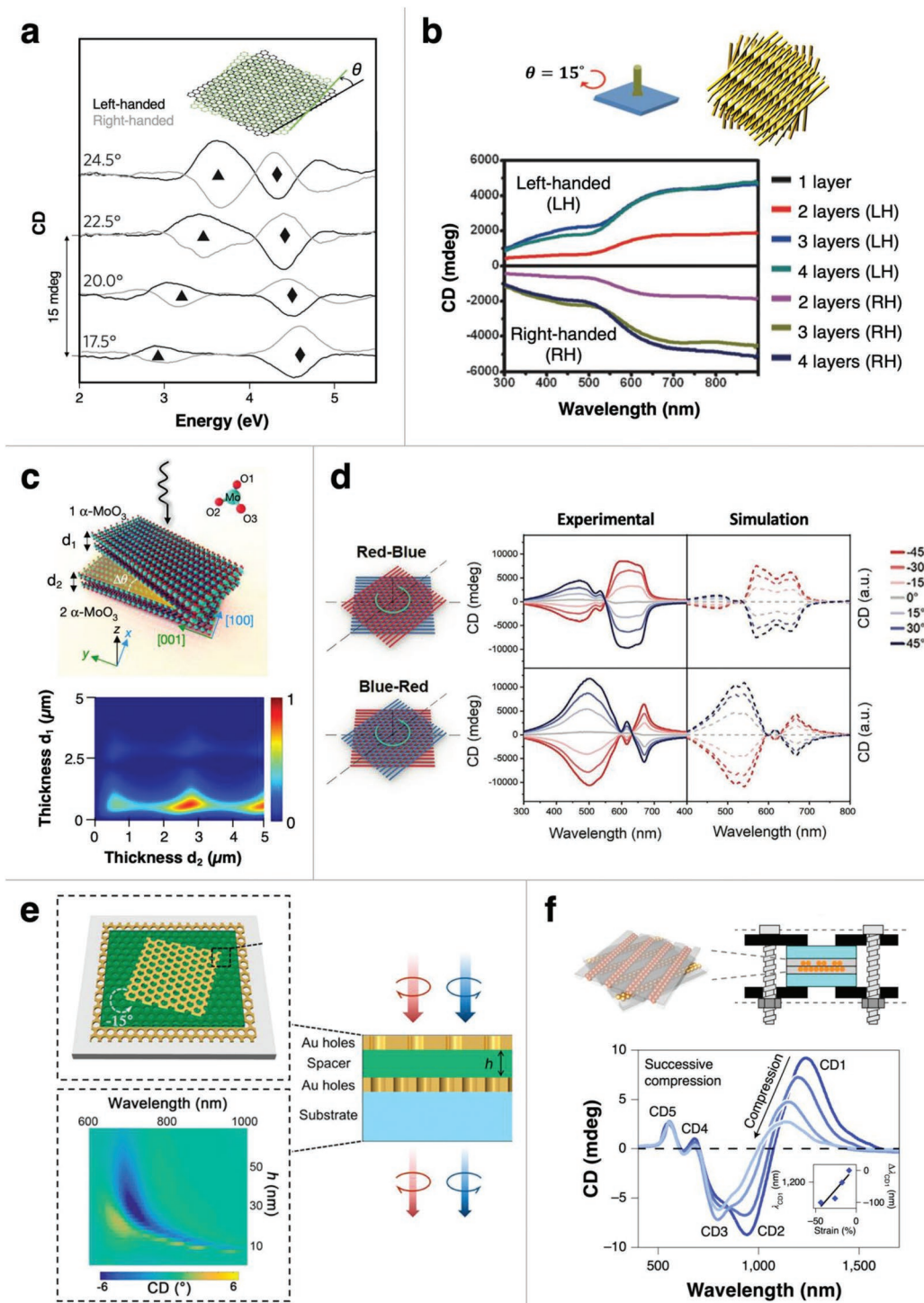


Figure 9. Tunable CD signals in planar chiral twisted metasurfaces at normal incidence. a) By changing the twist angle: CD spectra of twisted bilayer graphene. Adapted with permission.^[10] Copyright 2016, Springer Nature. b) By changing the layer number: CD spectra of twisted thin films of aligned Au nanowires with a fixed common interlayer twist angle of $\pm 15^\circ$. Reproduced with permission.^[15] Copyright 2017, Wiley-VCH. c) By changing the thickness of one or more layers. Scheme of twisted bilayer α -MoO₃ with top and bottom slab thicknesses of d_1 and d_2 , respectively. Reproduced with permission.^[27] Copyright 2020, Springer Nature. Heatmap showing the CD signal of 70° -twisted bilayer α -MoO₃ at a wavelength of $14.4 \mu\text{m}$. Reproduced with permission.^[14] Copyright 2021, IOP Publishing. d) By switching the stacking order in a twisted heterobilayer system: CD spectra of differently stacked layers of aligned polydiacetylene thin film in red and blue phases. Reproduced with permission.^[42] Copyright 2022, Wiley-VCH. e) By adding a dielectric interlayer and changing its thickness. Scheme and CD heatmap of a -15° -twisted bilayer Au nanohole arrays with a fibroin interlayer. Adapted with permission.^[139] Copyright 2018, American Chemical Society. f) By introducing mechanical strain into elastic film structure: applying a compressive force normal to the stacking plane of a -45° -twisted bilayer of AuNP dimer chain arrays in a polydimethylsiloxane template. Reproduced with permission.^[16] Copyright 2021, Springer Nature.

the impinging light play an important role in determining the chiroptical activity of flat chiral metasurface. First, changing the monolayer thicknesses in a twisted bilayer (or effectively double multilayer) tunes the observed CD. Taking twisted α -MoO₃ slabs, e.g., when the thicknesses of the two anisotropic layers were varied continuously from 0 to 5 μm , the highest CD signals were achieved when the top and bottom layers are 0.6 and 2.7 μm in thicknesses for several twist angles investigated (Figure 9c).^[14] Simply reversing the top and bottom layers would have an effect on the CD response as well. Polydiacetylene is a responsive polymer that undergoes a chromatic transition upon environmental change such as heating, thus resulting in two distinct phases known as the blue phase and the red phase. Twisted stacking of aligned polydiacetylene nanofibril thin films, therefore, makes possible the tunable and potentially switchable CD spectra. As shown in Figure 9d, the two heterobilayer stacking configurations produced distinct CD spectra. Importantly, the authors established that the CD spectra of red–blue heterobilayer resembled those of blue–blue homobilayer; similarly, the CD spectra of blue–red heterobilayer resembled those of red–red homobilayer.^[42] This study brings forth key insights into the role of the top layer in a chiral bilayer metasurface.

Since the origin of optical chirality stems from the twisted structural configuration, inserting a relatively thin dielectric interlayer does not negate the optical chirality of the metasurface. Changing the interlayer separation distance effectively modulates the coupling between the layers in a chiral metasurface—whether it is the metal–dielectric–metal near-field coupling in a plasmonic metasurface or near-field coupling between dielectric resonators in an all-dielectric metasurface. For periodic arrays of Au nanoholes, the twisted bilayer can support surface plasmon polaritons on its surface.^[18] When a dielectric medium is inserted between the layers, internal surface plasmon polaritons or gas surface plasmons are generated in the interlayer region and enables near-field coupling between layers (Figure 9e).^[139] This greatly enhances the CD signal from 0.2° in a bare homobilayer to 6° when a 30 nm dielectric is in place, corresponding to a nearly 30 times improvement. Similar enhancements were observed when comparing the bilayer metasurface with and without a dielectric spacer, with examples seen in Figure 8. For multiple twisted metasurfaces, numerical simulations confirmed that the electric, magnetic, and superchiral fields were concentrated and preferentially localized at the chiral interface or in the interlayer region.^[16,18,139,150] The thickness of the interlayer dielectric also affects the chiroptical signal, which has been demonstrated for metasurfaces of graphene nanoribbon arrays,^[114,151] aligned plasmonic nanowires,^[17] nanohole arrays,^[139] nanoantenna arrays,^[124] and single triskelion element.^[106] Another consideration is that the interlayer spacing can be engineered to match the helical feature of the circularly polarized incidence in order to modulate light–chiral matter interactions.^[152]

Last, for certain mechanically flexible metasurfaces, strain engineering allows reversible modulation of the CD spectra. A successful demonstration is shown in Figure 9f for a soft-template chiral plasmonic metasurface.^[16] The mechanism of mechano-tunability is based on the nanoparticle reconfiguration within the metasurface when the bilayer is bent to varied

degrees. While this strategy is fairly novel for chiral twisted metasurfaces, programming CD response through mechanical strain has been reported for similar chiroptical nanocomposites.^[140] Contrariwise, when investigating the effect of strain on twisted aligned nanofibril thin films on a flexible polyvinyl alcohol strip, Xie et al. found that there was minimal effect of the bending strain on both absorption and CD characteristics, which hints at durable performance in strain-sensitive applications.^[42]

While this review has focused on the optical chirality of twisted metasurfaces at normal incidence, shining light at an oblique angle might influence the measured chiroptics. For chiral 2D TBG or twisted bilayer α -MoO₃ crystalline slabs, their CD spectral responses have been found to remain relatively invariant with changing angles of incidence.^[10,14] However, achiral single-layer plasmonic nanohole arrays as well as metasurfaces with split ring apertures have shown pseudo-CD signals when light is obliquely illuminated onto the arrays.^[9,153,154] Hence, a twisted layered structure of these materials at oblique incidence would possess optical chirality of two different origins, generating an overall enhanced CD response. This superimposition was recently demonstrated by Lai and colleagues in a 90°-twisted bilayer metasurface comprising split ring resonator arrays (Figure 10).^[21]

To briefly sum up, ultrathin chiral metasurfaces fabricated from twisted stacking possess programmable chiral optical activities at normal incidence. Spectral features including the sign, magnitude, and spectral position of CD could be modulated by changing the interlayer twist angle, interlayer spacing, layer number, and so on. The flexible programmability is overall enabled by the additional degrees of freedom in comparison with traditional chiral metamaterials. Furthermore, most of the strategies for tuning CD as discussed above are broadly applicable to a large selection of materials systems, taking, e.g., the interlayer spacing that influences the coupling strength like electronic coupling of twisted 2D bilayers or near-field effects of plasmonic metasurfaces. Certain metasurface designs display real-time CD tunability by exploiting strain-induced reconfiguration, which is generally impossible for other artificial materials. Using obliquely incident light, the secondary extrinsic chirality could enhance the CD signal from the chiral metasurface, and thus the angle of incidence of light adds to an already-complex parameter space for tuning chiroptical performance. Future research is desired to investigate the interplay between the two forms of CD responses and to exploit this for advanced light manipulation. What is more, despite the diversity of the strategies, most have only been explored for a few disparate designs or systems. Fundamental insights and an overarching theoretical framework of the tunability of CD responses are still prerequisites for on-demand design of ultrathin chiral metasurfaces.

4. Chiroptical Applications of Chiral Twisted Metasurfaces

4.1. Polarization Rotators and Circular Polarizers

Optical technologies have laid the foundation for the Information Age. Despite numerous engineering feats such as

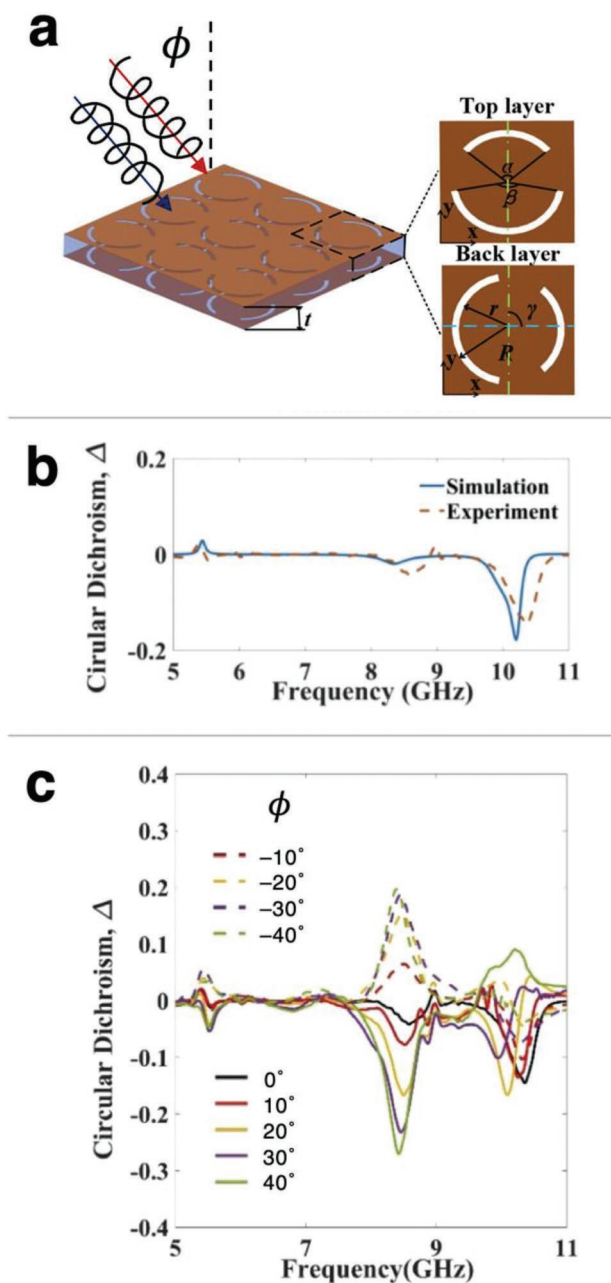


Figure 10. Enhanced CD in chiral metamaterials under oblique illumination. a) Design of 90° -twisted bilayer metasurface of split ring resonators separated by F4B PCB. b) CD of metasurface at normal incidence. c) CD of metasurface at oblique incidence of various angles. Reproduced under terms of the CC-BY license.^[21] Copyright 2020, The Authors, published by Optical Society of America.

the developments of optical fibers and ultrafast lasers, there is still an ultimate need to devise optical devices with control over the polarization, phase, and amplitude of electromagnetic waves. For instance, a twisted trilayer metasurface of split ring resonators was reported to be capable of independent control of polarization, phase, and amplitude.^[102] A successful demonstration of the multiplex beam wavefront shaping was also delineated. Recently, Overvig et al. put forward a Fano-based

twisted stacked metasurface leveraging quasi-bound states in the continuum capable of tailored phase control while encoding arbitrary polarization states.^[147] For pure polarization control, which is important for telecommunication or optical data storage applications,^[155–157] mechanical rotating devices such as waveplates are commonly used. Optical metadevices based on microelectromechanical systems have also been proposed for active polarization control.^[158] Nevertheless, much simpler designs that offer fabrication-related advantages are found in chiral stacked metasurfaces. Herein, chiral metasurfaces in nanoscale dimension for the control of linearly polarized and circularly polarized electromagnetic incidences are discussed, respectively.

When linearly polarized light is shone onto a polarization rotator, the polarization axis of the incidence is rotated, a phenomenon characterized by ORD. **Figure 11a** shows the design and chiroptical performance of a 22.5° -twisted bilayer plasmonic hole array as a polarization rotator.^[152] With a total device thickness of 110 nm, the average maximum optical rotation coefficient, also called thickness-normalized optical activity, was determined to be $2 \times 10^6 \text{ deg mm}^{-1}$. Similar but opposite chiroptical responses were recorded for the other enantiomer. Moreover, increasing the optical power of the incident beam allowed modification of the polarization control, either ORD or CD, in the chiral metasurface, i.e., the chiral metasurface exhibited tunable optical nonlinearity. The nonlinear optical rotation coefficient was $\approx 180 \text{ cm}^{-1} \text{ W}^{-1}$, which was orders of magnitude higher compared to commercially used materials such as lithium iodate (LiIO_3) crystals.^[152] Additionally, twisted arcs as plasmonic nanoantennae were designed for polarization conversion of linearly polarized light in the near-IR regime.^[110] Compared to plasmonic chiral metasurfaces, all-dielectric metasurfaces that enjoy significantly lower dissipative losses are more attractive as optical metadevices. Tanaka et al. designed a silicon-based all-dielectric chiral metasurface with a maximum optical rotation coefficient of $\approx 2.7 \times 10^5 \text{ deg mm}^{-1}$.^[101] Despite high optical rotation activities, the discussed chiral metasurfaces have a limited range of operational wavelengths, remaining to be further extended in order to achieve broadband wireless communications.^[159]

Broadband circular polarization was realized in a twisted AuNR-array metasurface.^[20] As expected, the optical performance of this chiral metasurface was tunable by changing the twist angle, the interlayer spacer thickness, or the layer number (**Figure 11b**). The authors also ascertained that the robustness of the broadband design was retained across the different metasurfaces, and the transmission characteristics were invariant even when laterally displacing one of the layers, suggesting the minimal effects of potential misalignment errors.^[20] Similarly, twisted stacked Al nanogratings also presented broadband CD, with an extinction ratio as high as 8, in the visible-near-IR range.^[160] Although comparable performances were recorded for the two metasurface designs, the latter might be more attractive. First, from a fabrication standpoint, nanograting can be facily prepared using nanoimprint lithography, whereas the nanorod arrays require more precise lithographic patterning. Second, Al is one of the elements that are directly mined with high global production,^[161] representing a more economic and sustainable alternative to precious metals like Au.

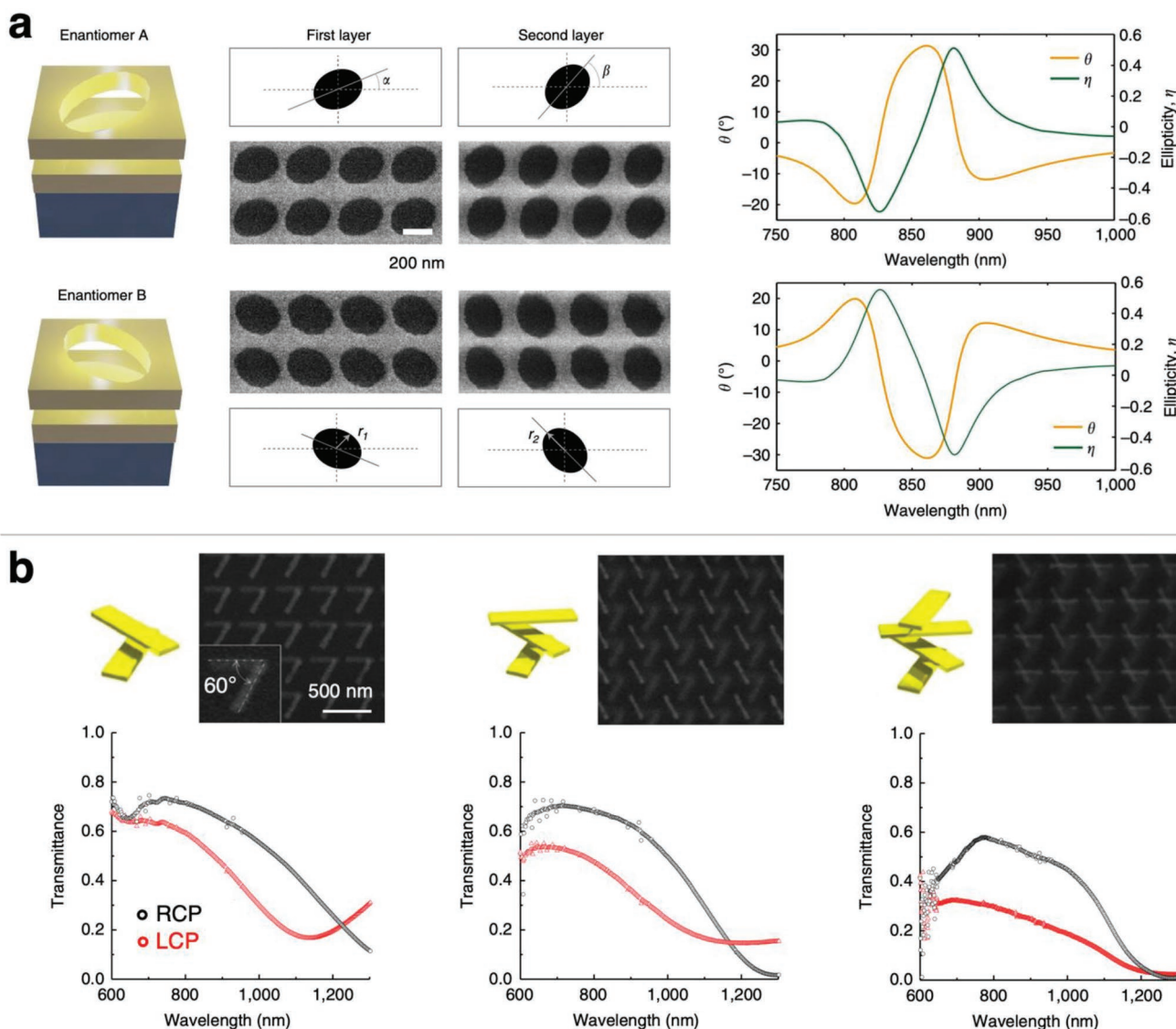


Figure 11. Chiral metasurfaces for polarization discrimination and control. a) Chiral metasurfaces based on 22.5°-twisted bilayer elliptical Ag hole arrays. The two enantiomers are labeled A and B. Corresponding ORD, measured as the polarization rotation angle, and CD spectra in the linear regime. Reproduced under terms of the CC-BY license.^[152] Copyright 2017, The Authors, published by Springer Nature. b) Broadband circular polarizers based on 60°-twisted layered AuNR arrays with layer numbers 2, 3, and 4, respectively. Stacking scheme, electron micrograph, and corresponding polarization-sensitive transmission profiles. Adapted under terms of the CC-BY license.^[20] Copyright 2012, The Authors, published by Springer Nature.

4.2. Polarization-Sensitive Optical Devices

Chiral metasurfaces possess absorption or transmission spectra that are sensitive to the polarization state of incident light. In its simplest form, the asymmetric transmission behavior may be utilized to construct optical filters that block light of a specific frequency or wavelength in a polarization-dependent manner. This property has been demonstrated in chiral metasurfaces comprised of twisted nanorod dimer arrays,^[125,162] twisted semi-circle arrays,^[124] or twisted circular disk arrays.^[163] Notably, for the AuNR-based chiral metamirror, the optical absorption spectrum under RCP light remains relatively unchanged regardless of the angle of incident light, suggesting the robust performance of the device for real-life applications as optical filters.^[162]

On the other hand, for polarization-independent optical filters, ultra-narrowband filters with a notch filter line shape can be achieved in a bilayer photonic slab, where the frequency to be filtered is tuned by simply changing the twist angle.^[43]

In the visible region, the differential transmission of LCP and RCP light might be exploited to enable color displays or color prints for data encryption. Xie et al. fabricated twisted homo- and heterobilayers of polydiacetylene thin films in the blue and red phases as flexible color display units.^[42] Based on the stacking configuration, each bilayer unit operated as a switch for the prime colors red, green, and blue in a one-to-one correspondence according to the polarization state of incident light (Figure 12a). Albeit a simple design, the polymeric chiral metasurface already covered $\approx 51\%$ of the maximum possible

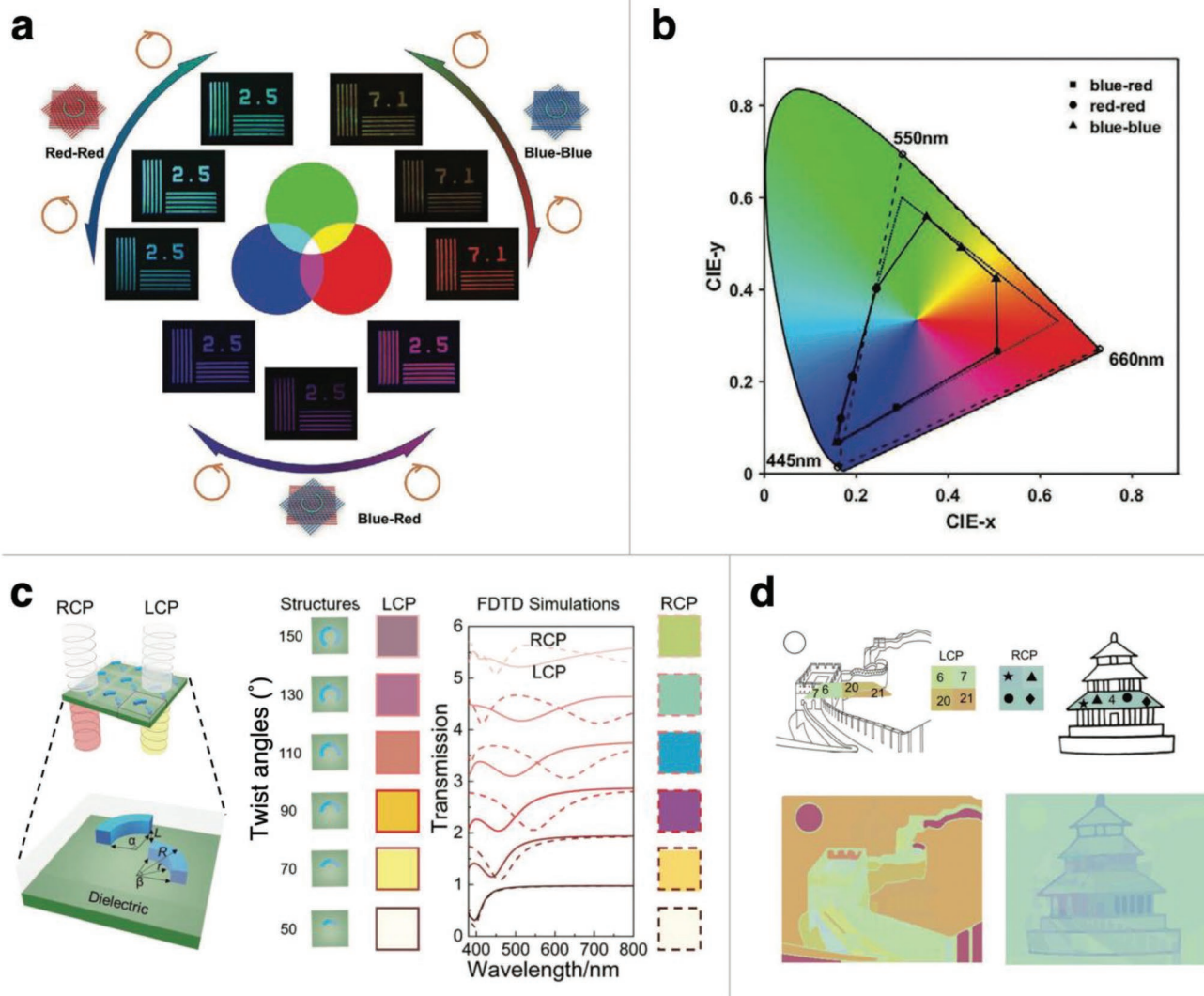


Figure 12. Chiral metasurfaces for color displays and encrypted color prints. a,b) Flexible multiplex color display based on 45°-twisted bilayers of polydiacetylene thin films. a) Selective color filtering performance of metasurface for LCP and RCP incident light. b) Corresponding color space chromaticity diagram showing the gamut of twisted metasurface. Reproduced with permission.^[42] Copyright 2022, Wiley-VCH. c,d) Counterfeiting color prints. c) Transmission spectra of LCP and RCP light through a twisted Al arc-based bilayer structure at different angular orientations. d) Chiral color prints showing two different encoded images under LCP and RCP light, respectively. Reproduced with permission.^[126] Copyright 2019, Royal Society of Chemistry.

gamut (Figure 12b), equal to $\approx 80\%$ of the capacity achievable by a typical sRGB color space. Compared to traditional color displays such as those based on liquid crystals, there are numerous potential advantages if current metasurfaces are further optimized. First, traditional liquid crystal displays rely on the physical alignment of molecules under an external field, a process that is known to suffer from slow responsivity at low operating temperature. The chiral metasurface design, in general, does not have this limitation. Second, different colors would be obtained without sacrificing much brightness of the output, which may be further improved by engineering the transmission characteristics of chiral metasurface. Most importantly, the polymeric chiral metasurface can be deposited onto a flexible substrate, acting as flexible color display units.^[42]

Data security through optical information encryption or optical counterfeiting measures is another active research topic in chiral metamaterials. One example is CD spectroscopy coding.^[76] However, this approach requires a spectral readout, and a large library of datasets may be needed for meaningful interpretation. Direct visual readout based on colors or images thus represents a simpler and more appealing alternative. Figure 12c shows how a bilayer stacking of twisted Al arcs generates distinct colors under LCP and RCP irradiations. Using these units as pixels, researchers were able to construct color prints with optical images that were only discerned for a specific polarization state of light beam (Figure 12d). Circularly polarized luminescence of materials-specific chiral bilayers also enables similar optical encryptions.^[42] A recent study using metasurfaces based on periodically repeated clusters

of meta-atoms reported the vectorial holographic encryption of data in a dual-band manner covering the UV and visible region.^[109]

4.3. Chemical and Biological Sensing

Chiral nanostructures with a large chiroptical response have long been sought for enantiodiscrimination of chiral compounds. One technologically relevant area is the quality control of medications, and their enantiomeric purity is of vital importance for achieving the intended pharmacological outcome.^[164–166] In pharmaceutical companies, optical polarimetry presented by CD is commonly used. Chiral metasurfaces that amplify light–matter interactions are able to improve the signal-to-noise ratio and decrease the detection limit for small molecule enantiomers. Most studies rely on a shift in the CD spectral peaks or dips, i.e., $\Delta\lambda$, when comparing the chiroptical signals of chiral metasurface with and without the analytes. This far-field spectral shift is believed to originate from the near-field interactions between small molecules and chiral substrate.^[119,167]

Using the twisted bilayers of plasmonic nanohole arrays, researchers successfully detected the drug molecule thalidomide adsorbed onto the metasurface and differentiated the two enantiomeric forms, where (S)-thalidomide was supposedly teratogenic in nature.^[18] The same metasurface platform was also used for clinical diagnosis of diseases, for which the associated biomarkers had a distinct chiral signature—in this case, L- versus D-glucose—in a label-free manner. A detection accuracy of 84% was obtained for clinical urine samples from diabetic patients with an ultralow sample volume requirement (10 μ L).^[168] Specifically, a microbubble technique was employed to induce prompt accumulation of L- or D-glucose onto the metasurface for rapid testing. To implement rapid and continual screening, a microfluidic or nanofluidic device geometry is desired. By incorporating a flow setup on top of a plasmonic nanorod-based chiral metasurface, solutions or suspensions containing chiral species were continuously monitored (Figure 13a).^[19] The authors considered the ensemble of chiral molecules sitting on the top of plasmonic chiral metamaterial and derived an expression for the total CD response. Following removal of the background signal, CD response of the chiral analytes was detected with high sensitivity up to zeptomole (10^{-21} mol) level.^[19]

Twisted bilayer metasurfaces have been shown to possess concentrated superchiral fields at the chiral interface according to field simulations,^[16,18] whereas they localize at the surface on the incidence side for similar monolayer nanostructures.^[130] These near-fields amplify the optical signal of small molecules, thus helping achieve their detection with high sensitivity. Using this information, researchers deposited biomolecules such as proteins in the interlayer region prior to twisted stacking, whereby ultrasensitive biosensing of proteins is realized (Figure 13b).^[16] For practical exploitation of the superchiral field between the twisted layers, microfluidic channels can be incorporated into the interlayer dielectric for flow-cell-based analysis.

The deployment of stimuli-responsive materials provides an ingenious route for chiral metasurface designs for

broad-spectrum environmental sensing applications beyond chirality sensing. For example, fibroin silk undergoes microstructural alterations with noticeable swelling or shrinkage behaviors when immersed in different solvents. When used as an interlayer spacer, such alternations, which affect the interlayer spacing as well as the intrinsic optical properties of the interlayer medium, were reflected in the change in CD spectra. The stimuli-specific response enables the detection of trace concentrations of solvent impurities. Figure 13c illustrates how the solvent polarity modulated the interlayer properties, leading to CD spectral change that was used for detecting water residues in isopropyl alcohol.^[139] Similarly, methanol impurities as low as 0.02% in hexane were also discerned.^[139]

Besides CD spectra, reflection responses have been also exploited for sensing applications. Using a twisted bilayer metasurface with I-shaped inclusions, Zhang et al. leveraged the change in the reflection signals from circular polarization spectroscopy to monitor the thermal denaturation of proteins at terahertz frequencies.^[99] Different trends in the reflection spectral change were detected for three different common proteins at varying degrees of denaturation. This study showed the potential applicability of this metadvice for terahertz protein quality control in the biotechnology or food industries.

Overall, compared to other chiral nanostructures such as chiral Au nanoparticle suspensions, chiral stacked thin films possess numerous advantages in sensing applications. First, it is easy to deposit the analyte onto the planar metasurface. The chemicals to be analyzed can be deposited via simple drop-casting, whereas thorough mixing with nanostructures in a confined vial is needed for colloidal-based chiral sensors. The use of a microfluidic flow cell further helps automate the process for industrial implementation of chiral metasurface polarimetric devices. Second, the analytes might be either solution-based or solid-states (e.g., in powder form), whereas analytes in powder form must be dissolved into the specific solvent using the colloidal-based chiral sensors. Third, as an immobilized metasurface optical device, if there is no or negligible interlayer entrapment of analytes, chiral metasurfaces enjoy high reusability as a sensing platform. Actually, the chiral metasurface with a flexible polydimethylsiloxane substrate by Probst et al. permitted rotational reconfigurability and deformability for setting-specific sensing applications.^[16]

4.4. Toward Hybrid Metadevices

Apart from the direct application as optical or opto-sensing devices, a chiral metasurface has been become a versatile platform to construct hybrid metadevices. Quantum valleytronics, first introduced in 2007, has attracted much attention for its potential use in information encodement and processing.^[169] Local valleys in the electronic band structure of a semiconductor possess distinctly identifiable energies or momenta, and their manipulation has direct implications for electronic logic in quantum computing.^[170] In a study from 2019, a semiconducting WSe₂ monolayer was inserted into the interlayer region of a plasmonic chiral metasurface, whereby the interaction of valley excitons and the superchiral field in optical cavities was exploited to modulate the valley dynamics of the

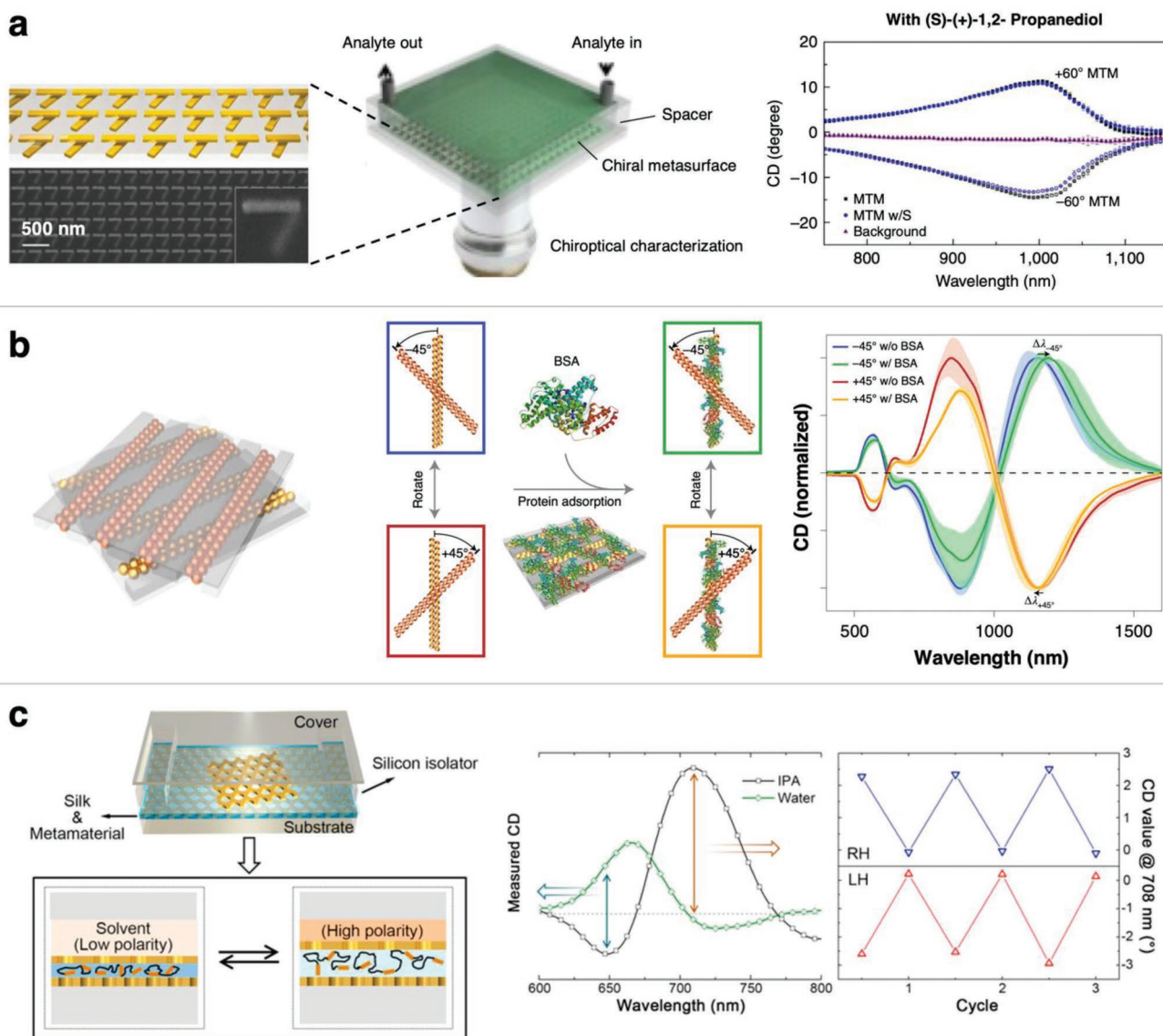


Figure 13. Chiral metasurfaces for chemical and biological sensing. a) High-sensitivity detection of chiral metabolites in a flow-cell setup using twisted bilayer AuNR arrays. Processed CD spectra for analytes upon removal of background metamaterial CD signals. Adapted upon terms of the CC-BY license.^[19] Copyright 2017, The Authors, published by Springer Nature. b) Enhanced chiral sensing of protein bovine serum albumin (BSA) in the interlayer region of a chiral bilayer plasmonic film. Reproduced with permission.^[16] Copyright 2021, Springer Nature. c) Environmental sensing using a nanohole-array-based chiral metasurface with a fibroin interlayer. CD spectra showing reversible chiroptical signals when exposing the silk-metamaterial to water and isopropyl alcohol (IPA) alternatively for three cycles. Reproduced with permission.^[139] Copyright 2018, American Chemical Society.

2D monolayer.^[171] Shown in **Figure 14a**, the metadvice has the WSe₂ monolayer placed above a dielectric spacer and altogether sandwiched between two layers of nanohole arrays stacked at an angle. The total device thickness is <130 nm, corresponding to around one-sixth of the operational wavelength. When the metasurface is achirally stacked, either as an untwisted or 30°-twisted bilayer, there is no difference between the polarization-resolved photoluminescence spectra. In contrast, for the two enantiomeric stacking configurations, there is distinct valley-polarized emission with its sign determined by the handedness of the metasurface owing to the chiral Purcell effect (**Figure 14b**). Such hybridization of valley dynamics

and optical cavities with enhanced electromagnetic near-fields (**Figure 14c**) offers a convenient approach to engineer the optics of 2D excitonic nanostructures and more generally valleytronic devices under ambient condition. Although similar chiral near-fields have been exploited for this purpose,^[172,173] the twisted bilayer stacking geometry enabled additional tunability of the spectral position of circular polarization emission by either changing the twist angle of plasmonic metasurface or by increasing the dielectric spacer thickness. There are also additional advantages of this design principle. First, sandwiching 2D monolayer in the chiral metasurface effectively shields the emission medium, offering environmental

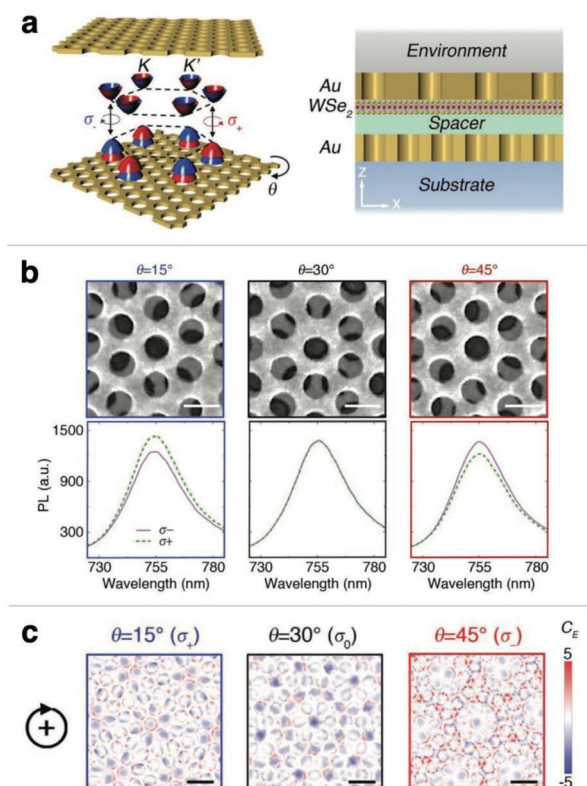


Figure 14. Modulation of excitonic dynamics in 2D monolayer using a plasmonic chiral metasurface. a) Hybrid metadvice: scheme of WSe₂ valley dynamics modulation and metadvice geometry. b) SEM images showing top view and corresponding polarization-resolved photoluminescence spectra of the hybrid metamaterials with different interlayer twist angles. Scale bars = 300 nm. c) Corresponding simulated superchiral fields at the plane of the 2D monolayer. Scale bars = 1 μ m. Reproduced with permission.^[177] Copyright 2019, Wiley-VCH.

protection against parasitic surface contaminants. As a proof of concept, the WSe₂-plasmonic chiral metasurface hybrid was shown to display nearly reversible ON/OFF switching of the valley-polarized emission in water and in air under cyclic experiments.^[171] Second, previous methods for controlling the valley-polarized emission of a single layer of transition metal dichalcogenide include the application of an electrical bias and optical pumping;^[174,175] however, both approaches rely on carrier injection to create disproportionate valley populations. The employment of chiral metasurfaces proposed by Wu et al. is solely based on chiral-selective light–matter interactions. Third, it is a straightforward approach by comparison and does not require cumbersome device fabrication or specialized optical equipment.

5. Outlook

Ultrathin chiral metastructures are gaining ground at a rapid pace; nevertheless, the research on chiral twisted metasurfaces is still in its infancy. Here, we offer the perspectives on the

future research directions in these subwavelength nanostructures from three different aspects—materials and design, fundamental properties and emergent phenomena, and advanced applications—and discuss their broad impacts.

5.1. Materials and Metasurface Design

Chirality, though prevalent in nature, has mostly been made tunable with engineered constructs. Twisted chiral stacking of nanostructures offers one promising way of switching and modulating the optical chirality. However, current chiral metasurfaces in the literatures are focused on a limited selection of nanomaterials systems, some of which are not yet experimentally realized. Expanding the materials toolkit will not only help identify high-performance metasurfaces and greatly accelerate their translation toward practical applications, but also afford a viable platform for discovering novel helicity-selective effects. Looking at 2D materials, their ultrathin dimensions mean that the quantum mechanical nature of the quasi-particles like electrons and polaritons become more relevant in light–matter interactions, leading to ultraconfined optical fields.^[176] Moreover, while there is an explosion of studies on twisted bilayers of graphene and transition metal dichalcogenides in recent years, other low-dimensional nanostructures with intrinsically high absorptivity such as MXene^[177] and perovskite^[178] deserve to be investigated, for instance, to attain ultrahigh thickness-normalized ellipticity. We also envision new research on the twist engineering of these emergent 2D materials upon chiral stacking. Nevertheless, the key challenge for twisted stacked 2D thin films lies in the preparation of large-area, single-crystalline monolayers and, for patterned 2D materials, advanced nanofabrication with suitable transfer methodologies.

Manipulating the nanoscale structures has profound implications in tailoring light–matter interactions, as seen in the significant strides made for antenna-based metasurfaces. Most chiral stacked nanomaterials discussed employ simple achiral monolayers, and some lack nanoscale resonant structures. Intrinsically chiral nanostructures^[8]—such as those coated with chiral ligands or possessing chiral morphologies—can be used as constituent components to further engineer light–matter interactions at the nanoscale. They can self-assemble into superlattices that act as a monolayer, and the resultant twisted stacked metasurfaces are expected to possess hierarchical and multiscale chirality from the nanoscale to the mesoscale, endowing tunable chiroptics via changing single-unit chirality in the metasurface. Depending on the direction of incidence, orientationally anisotropic CD responses would be observed using this approach. From a fabrication point of view, self-assembly being an energy-efficient process compared to lithography-intensive fabrication is desirable for preparing metasurfaces, though additional work is needed to address the scalability problem.^[179]

Regardless of the materials system, the predictable design of chiral optics and photonics remains a challenge in the field. Although some inverse design approaches exist,^[103,180] it is difficult to establish tangible, intuitive correlations between structure/design and chiral optical activity, especially considering the multidimensional parameter space for the chiral

metasurfaces. To tackle this, machine learning emerges as an alternative method for accelerating parameter optimization. Using two bidirectional neural networks, it is possible to create high-performance chiral metasurfaces with predesignated resonant frequency and bandwidth.^[103] Depending on the number of input performance metrics, machine learning methods could produce multiple sets of possible design parameters, endowing flexibility in fabricating chiral metasurfaces for real-world applications.

5.2. Fundamental Properties and Emergent Phenomena at the Chiral Twisted Interface

In addition to steady-state optical chirality, twist-dependent and chiral-selective properties of ultrathin layered nanostructures are awaiting full exploration. First, there are limited fundamental insights on superchiral fields that concentrate at the interlayer region of a chiral bilayer metasurface. Despite extensive numerical simulation of this near-field effect and its exploitation for sensing applications, the tunability and spatial distribution for multilayer chiral structures are largely unexplored. Our understanding of this superchiral field is also mostly limited to the linear regime. Second, twisted stacked metasurfaces composed of graphene nanoribbons or α -MoO₃ slabs display photonic dispersions that are modulated via the interlayer twist angle.^[25,27,181] At the “photonic magic angle,” broadband field canalizations are realized where the polariton-coupled dispersions become essentially flat. These Moiré-enabled twist-photonics and -polaritonics could find applications in nanoimaging and radiative energy control. As many hyperbolic metamaterials have been found,^[182] they might be used to explore such photonic topological transitions in other frequency ranges, which is of significance for fundamental science and advanced applications. Third, optical nonlinearities have only been briefly studied in chiral metasurfaces and deserve more in-depth investigations.^[4,152,183–185] Nonlinear optics are pivotal for lasing technologies, optical computing and processing, and ultrafast switches;^[186] and new possibilities for quantum nanophotonics could unfold by leveraging nonlinear optical processes. Valev and colleagues designed subwavelength chiral metasurface with large SHG CD (>0.5),^[187] which may prove useful for establishing optical autocorrelation for measuring ultrashort chiral laser pulses. Ultrathin chiral metasurfaces with their planarized geometry and controllable chiroptics could act as integrated all-optical processing systems with high polarization sensitivity. Finally, twisted stacking has enabled the field of 2D twistronics to emerge, leading to twist angle-dependent properties beyond optical activity. Chiral stacked 2D materials possess exotic Moiré optics and novel electronic properties, whereby opposite stacking configurations of an identical 2D system may possess distinct topological and transport behaviors.^[188,189] When two atomically thin periodic lattices are superimposed on top of each other, Moiré patterns with uniquely tunable potential landscapes emerge. Due to programmable electron localization that gives rise to artificial atoms, these Moiré 2D materials have been used as quantum simulators to probe quantum mechanical phenomena elusive to conventional materials.^[28,189] Understanding the relevance

and importance of stacking chirality on these twisted 2D materials will provide key insights into phenomenon such as chirality-induced spin selectivity, magneto-chiral anisotropy and quantum transport.

5.3. Advanced Applications of Ultrathin Chiral Metasurfaces

As already discussed extensively in this review, there are numerous application areas for chiral twisted metasurfaces with subwavelength thicknesses, including light polarization control, metasurface-enhanced chiral spectroscopies, and optical encryption. Below we list out some potential advanced optical applications and future areas for exploration. First, current chiral twisted metasurfaces have shown some potential of optical information processing in the visible range, yet the bandwidth of the CD response is not always designable. A recent study demonstrated that optical skyrmions displaying sharp, multiresonant, and equidistant eigenmodes were observed in an ultrathin mirror-symmetry-breaking metasurface.^[190] Such resonant operable modes would be useful for high-precision optical processing across a wide frequency range. Second, the innovation on material and design certainly benefits the use of ultrathin chiral metasurfaces as planarized metadevices with multiple functionalities. For example, chiral TBG enjoys high electrical conductivity^[191,192] and twist-angle-tunable electrochemical signatures^[193] in addition to optical chirality. By simultaneously leveraging twist-engineered electronic and optical properties, chiral twisted 2D materials may soon find applications in polarization-based electro-optical metadevices. Lastly, stimuli-responsiveness in ultrathin chiral metasurfaces could provide multiple application opportunities. Devices used for space exploration, for instance, require ultra-compactness for storage and stimuli-responsiveness in order to be deployed remotely in outer space in an on-demand fashion. It is certainly possible to construct reconfigurable and stimuli-responsive chiral metasurfaces using inspirations from origami and kirigami.^[194–196] The designed out-of-plane actuation would provide an extra degree of freedom for optical chirality control.

6. Conclusions

This review has surveyed the state-of-the-art studies on ultrathin chiral metasurfaces fabricated by rotationally aligning two or more layers of thin-film nanomaterials at an angle. Recent advances in materials systems and designs, fabrication methods, circular dichroic responses, and relevant applications have been discussed. Specifically, 2D vdW monolayers, nanowire-based thin films, antenna-based metasurfaces, and single-crystalline slabs have been stacked with an interlayer rotation to prepare chiral metasurfaces with subwavelength thicknesses. The induced chiral signature originates from the spatial twisting of the layers with a defined handedness to break mirror symmetry. For a given materials system, its chiral-optical signals are programmable via a variety of external means such as by changing the interlayer twist angle, adding a dielectric spacer, or modulating its thickness. Their ultrahigh chiroptical performance, as quantified by ellipticity and g-factor,

makes chiral twisted metasurfaces excellent candidates for use as circular polarizers, optical counterfeiting devices, metaholograms, color display units, and chiral sensing platforms. Their unique advantages compared to other metasurface devices and/or chiral nanostructures are also enumerated. On top of their direct application as optical devices, the potential of chiral twisted metasurface as a powerful platform for engineering the photodynamics of low-dimensional materials has been recently demonstrated. Even though rapid progresses have been made, we believe there is still plenty of room for improvement as well as new discoveries. Enhancements of the chiroptical performance like the CD magnitude could be made on current chiral metasurfaces. Additionally, these designs suffer from poor inverse designability, since it is not straightforward to correlate structure/design to chiroptical performance metrics including the operational wavelengths. Machine learning approaches are attractive in this regard, but an overarching theoretical framework of the design–property relationships in chiral metasurfaces is also needed. Beyond simple chiroptics, twisted stacking of ultrathin nanostructures provides a powerful platform for the discovery of novel optical and perhaps spin-selective phenomena with twist angle dependencies. With new advances in materials synthesis and nanofabrication strategies, future research on ultrathin chiral metasurfaces will open doors to new chiral nanostructure designs for use in diverse scenarios including ultrasensitive sensing and diagnostics, polarization-sensitive photonics and optoelectronics, and as planarized multifunctional metadevices.

Acknowledgements

The authors acknowledge the financial support from National Key R&D Program of China (2021YFA1200302 to Z.Y.T.), Strategic Priority Research Program of Chinese Academy of Sciences (XDB36000000 to Z.Y.T.), National Natural Science Foundation of China (92056204, 21890381, and 21721002 to Z.Y.T., and 21975060 to X.L.W.) and Youth Innovation Promotion Association CAS (2019039 to X.L.W.).

Conflict of Interest

The authors declare no conflict of interest.

Keywords

chiroptics, metadevices, polarization, thin films, twisted bilayers

Received: July 6, 2022

Revised: September 22, 2022

Published online: November 29, 2022

- [1] G. H. Wagnière, *On Chirality and the Universal Asymmetry*, Wiley-VCH, Weinheim, Germany **2007**.
- [2] J. T. Collins, C. Kuppe, D. C. Hooper, C. Sibia, M. Centini, V. K. Valev, *Adv. Opt. Mater.* **2017**, *5*, 1700182.
- [3] S. Li, J. Liu, N. S. Ramesar, H. Heinz, L. Xu, C. Xu, N. A. Kotov, *Nat. Commun.* **2019**, *10*, 4826.
- [4] G. Li, S. Zhang, T. Zentgraf, *Nat. Rev. Mater.* **2017**, *2*, 17010.

- [5] C. Hao, R. Gao, Y. Li, L. Xu, M. Sun, C. Xu, H. Kuang, *Angew. Chem.* **2019**, *131*, 7449.
- [6] W. Wu, M. Pauly, *Mater. Adv.* **2022**, *3*, 186.
- [7] M. Hentschel, M. Schäferling, X. Duan, H. Giessen, N. Liu, *Sci. Adv.* **2017**, *3*, e1602735.
- [8] J. Lv, X. Gao, B. Han, Y. Zhu, K. Hou, Z. Tang, *Nat. Rev. Chem.* **2022**, *6*, 125.
- [9] X. Wang, Z. Tang, *Small* **2017**, *13*, 1601115.
- [10] C. J. Kim, A. Sánchez-Castillo, Z. Ziegler, Y. Ogawa, C. Noguez, J. Park, *Nat. Nanotechnol.* **2016**, *11*, 520.
- [11] X. Zhang, Y. Zhong, T. Low, H. Chen, X. Lin, *Phys. Rev. B.* **2021**, *103*, 195405.
- [12] H. Ochoa, A. Asenjo-Garcia, *Phys. Rev. Lett.* **2020**, *125*, 37402.
- [13] H. Y. Lee, M. M. Al Ezzi, N. Raghuvanshi, J. Y. Chung, K. Watanabe, T. Taniguchi, S. Garaj, S. Adam, S. Gradečak, *Nano Lett.* **2021**, *21*, 2832.
- [14] B.-Y. Wu, Z. Shi, F. Wu, M. Wang, X. Wu, *Chin. Phys. B* **2022**, *31*, 044101.
- [15] J. Lv, K. Hou, D. Ding, D. Wang, B. Han, X. Gao, M. Zhao, L. Shi, J. Guo, Y. Zheng, X. Zhang, C. Lu, L. Huang, W. Huang, Z. Tang, *Angew. Chem., Int. Ed.* **2017**, *56*, 5055.
- [16] P. T. Probst, M. Mayer, V. Gupta, A. M. Steiner, Z. Zhou, G. K. Auernhammer, T. A. F. König, A. Fery, *Nat. Mater.* **2021**, *20*, 1024.
- [17] W. Wu, Y. Battie, V. Lemaire, G. Decher, M. Pauly, *Nano Lett.* **2021**, *21*, 8298.
- [18] Z. Wu, Y. Zheng, *Adv. Opt. Mater.* **2017**, *5*, 1700034.
- [19] Y. Zhao, A. N. Askarpour, L. Sun, J. Shi, X. Li, A. Alù, *Nat. Commun.* **2017**, *8*, 14180.
- [20] Y. Zhao, M. A. Belkin, A. Alù, *Nat. Commun.* **2012**, *3*, 1877.
- [21] P. Lai, G. Dong, W. Wang, T. Chen, T. Lv, B. Lv, Z. Zhu, Y. Li, C. Guan, J. Shi, *Opt. Express* **2020**, *28*, 15071.
- [22] J. K. Gansel, M. Thiel, M. S. Rill, M. Decker, K. Bade, V. Saile, G. Von Freymann, S. Linden, M. Wegener, *Science* **2009**, *325*, 1513.
- [23] J. K. Gansel, M. Latzel, A. Frölich, J. Kaschke, M. Thiel, M. Wegener, *Appl. Phys. Lett.* **2012**, *100*, 101109.
- [24] J. Kaschke, M. Wegener, *Opt. Lett.* **2015**, *40*, 3986.
- [25] G. Hu, A. Krasnok, Y. Mazor, C. W. Qiu, A. Alù, *Nano Lett.* **2020**, *20*, 3217.
- [26] A. V. Rogacheva, V. A. Fedotov, A. S. Schwanecke, N. I. Zheludev, *Phys. Rev. Lett.* **2006**, *97*, 177401.
- [27] G. Hu, Q. Ou, G. Si, Y. Wu, J. Wu, Z. Dai, A. Krasnok, Y. Mazor, Q. Zhang, Q. Bao, C. Qiu, A. Alù, *Nature* **2020**, *582*, 209.
- [28] D. M. Kennes, M. Claassen, L. Xian, A. Georges, A. J. Millis, J. Hone, C. R. Dean, D. N. Basov, A. N. Pasupathy, A. Rubio, *Nat. Phys.* **2021**, *17*, 155.
- [29] G. Tarnopolsky, A. J. Kruchkov, A. Vishwanath, *Phys. Rev. Lett.* **2019**, *122*, 106405.
- [30] Y. Cao, V. Fatemi, A. Demir, S. Fang, S. L. Tomarken, J. Y. Luo, J. D. Sanchez-Yamagishi, K. Watanabe, T. Taniguchi, E. Kaxiras, R. C. Ashoori, P. Jarillo-Herrero, *Nature* **2018**, *556*, 80.
- [31] J. Yan, W. Y. Ruan, M. Y. Chou, *Phys. Rev. B* **2008**, *77*, 125401.
- [32] F. Wang, Y. Zhang, C. Tian, C. Girit, A. Zettl, M. Crommie, Y. R. Shen, *Science* **2008**, *320*, 206.
- [33] P. Moon, M. Koshino, *Phys. Rev. B* **2013**, *87*, 205404.
- [34] E. S. Morell, L. Chico, L. Brey, *2D Mater.* **2017**, *4*, 035015.
- [35] F. Yang, W. Song, F. Meng, F. Luo, S. Lou, S. Lin, Z. Gong, J. Cao, E. S. Barnard, E. Chan, L. Yang, J. Yao, *Matter* **2020**, *3*, 1361.
- [36] J. Yin, H. Wang, H. H. Peng, Z. Tan, L. Liao, L. Lin, X. Sun, A. L. Koh, Y. Chen, H. H. Peng, Z. Liu, *Nat. Commun.* **2016**, *7*, 10699.
- [37] B. Deng, C. Ma, Q. Wang, S. Yuan, K. Watanabe, T. Taniguchi, F. Zhang, F. Xia, *Nat. Photonics* **2020**, *14*, 549.
- [38] K. Wang, B. Huang, M. Tian, F. Ceballos, M. W. Lin, M. Mahjouri-Samani, A. Boulesbaa, A. A. Puzos, C. M. Rouleau,

- M. Yoon, H. Zhao, K. Xiao, G. Duscher, D. B. Geohegan, *ACS Nano* **2016**, *10*, 6612.
- [39] W. Choi, I. Akhtar, M. A. Rehman, M. Kim, D. Kang, J. Jung, Y. Myung, J. Kim, H. Cheong, Y. Seo, *ACS Appl. Mater. Interfaces* **2019**, *11*, 2470.
- [40] X. Zhang, T. Wu, C. Yu, R. Lu, *Adv. Mater.* **2021**, *33*, 2104695.
- [41] X. Wu, C. Fu, Z. M. Zhang, *Opt. Commun.* **2019**, *452*, 124.
- [42] Y. Xie, P. Yang, L. Deng, Z. Feng, J. Li, C. Zhang, X. Tang, C. Li, J. Li, L. Xu, D. Zhang, X. Chen, G. Zou, *Adv. Opt. Mater.* **2022**, *10*, 2102197.
- [43] B. Lou, S. Fan, *ACS Photonics* **2022**, *9*, 800.
- [44] S. Carr, D. Massatt, S. Fang, P. Cazeaux, M. Luskin, E. Kaxiras, *Phys. Rev. B* **2017**, *95*, 075420.
- [45] T. Stauber, T. Low, G. Gómez-Santos, *Phys. Rev. Lett.* **2018**, *120*, 46801.
- [46] H. Xie, X. Luo, G. Ye, Z. Ye, H. Ge, S. H. Sung, E. Rennich, S. Yan, Y. Fu, S. Tian, H. Lei, R. Hovden, K. Sun, R. He, L. Zhao, *Nat. Phys.* **2022**, *18*, 30.
- [47] O. Can, T. Tummuru, R. P. Day, I. Elfimov, A. Damascelli, M. Franz, *Nat. Phys.* **2021**, *17*, 519.
- [48] H. Tan, C. Wang, H. Duan, J. Tian, Q. Ji, Y. Lu, F. Hu, W. Hu, G. Li, N. Li, Y. Wang, W. Chu, Z. Sun, W. Yan, *ACS Appl. Mater. Interfaces* **2021**, *13*, 33363.
- [49] F. Xia, H. Wang, D. Xiao, M. Dubey, A. Ramasubramaniam, *Nat. Photonics* **2014**, *8*, 899.
- [50] W. Xin, X. D. Chen, Z. B. Liu, W. S. Jiang, X. G. Gao, X. Q. Jiang, Y. Chen, J. G. Tian, *Adv. Opt. Mater.* **2016**, *4*, 1703.
- [51] W. Wang, A. Klots, D. Prasai, Y. Yang, K. I. Bolotin, J. Valentine, *Nano Lett.* **2015**, *15*, 7440.
- [52] G. Xu, D. Liu, S. Li, Y. Wu, Z. Zhang, S. Wang, Z. Huang, Y. Zhang, *Nano Res.* **2022**, *15*, 2689.
- [53] C. Ma, S. Yuan, P. Cheung, K. Watanabe, T. Taniguchi, F. Zhang, F. Xia, *Nature* **2022**, *604*, 266.
- [54] T. Latychevskaia, S.-K. Son, Y. Yang, D. Chancellor, M. Brown, S. Ozdemir, I. Madan, G. Berruto, F. Carbone, A. Mishchenko, K. S. Novoselov, *Front. Phys.* **2019**, *14*, 13608.
- [55] Z. Yan, Y. Liu, L. Ju, Z. Peng, J. Lin, G. Wang, H. Zhou, C. Xiang, E. L. G. Samuel, C. Kittrell, V. I. Artyukhov, F. Wang, B. I. Yakobson, J. M. Tour, *Angew. Chem.* **2014**, *126*, 1591.
- [56] H. Cho, Y. Park, S. Kim, T. Ahn, T. H. Kim, H. C. Choi, *npj 2D Mater. Appl.* **2020**, *4*, 35.
- [57] S. Xing, W. Wu, Y. Wang, J. Bao, S. S. Pei, *Chem. Phys. Lett.* **2013**, *580*, 62.
- [58] L. Sun, Z. Wang, Y. Wang, L. Zhao, Y. Li, B. Chen, S. Huang, S. Zhang, W. Wang, D. Pei, H. Fang, S. Zhong, H. Liu, J. Zhang, L. Tong, Y. Chen, Z. Li, M. H. Rummeli, K. S. Novoselov, H. Peng, L. Lin, Z. Liu, *Nat. Commun.* **2021**, *12*, 2391.
- [59] K. Liu, L. Zhang, T. Cao, C. Jin, D. Qiu, Q. Zhou, A. Zettl, P. Yang, S. G. Louie, F. Wang, *Nat. Commun.* **2014**, *5*, 4966.
- [60] S. Zheng, L. Sun, X. Zhou, F. Liu, Z. Liu, Z. Shen, H. J. Fan, *Adv. Opt. Mater.* **2015**, *3*, 1600.
- [61] M. Liao, Z. Wei, L. Du, Q. Wang, J. Tang, H. Yu, F. Wu, J. Zhao, X. Xu, B. Han, K. Liu, P. Gao, T. Polcar, Z. Sun, D. Shi, R. Yang, G. Zhang, *Nat. Commun.* **2020**, *11*, 2153.
- [62] W. Zhang, H. Hao, Y. Lee, Y. Zhao, L. Tong, K. Kim, N. Liu, *Adv. Funct. Mater.* **2022**, *32*, 2111529.
- [63] L. Cai, G. Yu, *Adv. Mater.* **2021**, *33*, 202004974.
- [64] K. Kim, M. Yankowitz, B. Fallahzad, S. Kang, H. C. P. P. Movva, S. Huang, S. Larentis, C. M. Corbet, T. Taniguchi, K. Watanabe, S. K. Banerjee, B. J. LeRoy, E. Tutuc, *Nano Lett.* **2016**, *16*, 1989.
- [65] S. Fan, Q. A. Vu, M. D. Tran, S. Adhikari, Y. H. Lee, *2D Mater.* **2020**, *7*, 022005.
- [66] S. Lan, X. Liu, S. Wang, H. Zhu, Y. Liu, C. Gong, S. Yang, J. Shi, Y. Wang, X. Zhang, *Nat. Commun.* **2021**, *12*, 2088.
- [67] H. Imamura, A. Visikovsky, R. Uotani, T. Kajiwara, H. Ando, T. Iimori, K. Iwata, T. Miyamachi, K. Nakatsuji, K. Mase, T. Shirasawa, F. Komori, S. Tanaka, *Appl. Phys. Express* **2020**, *13*, 075004.
- [68] C. Liu, Z. Li, R. Qiao, Q. Wang, Z. Zhang, F. Liu, Z. Zhou, N. Shang, H. Fang, M. Wang, Z. Liu, Z. Feng, Y. Cheng, H. Wu, D. Gong, S. Liu, Z. Zhang, D. Zou, Y. Fu, J. He, H. Hong, M. Wu, P. Gao, P.-H. Tan, X. Wang, D. Yu, E. Wang, Z.-J. Wang, K. Liu, *Nat. Mater.* **2022**, *21*, 1263.
- [69] H. Chen, X. L. Zhang, Y. Y. Zhang, D. Wang, D. L. Bao, Y. Que, W. Xiao, S. Du, M. Ouyang, S. T. Pantelides, H.-J. Gao, *Science* **2019**, *365*, 1036.
- [70] C. N. Lau, M. W. Bockrath, K. F. Mak, F. Zhang, *Nature* **2022**, *602*, 41.
- [71] E. Y. Andrei, A. H. MacDonald, *Nat. Mater.* **2020**, *19*, 1265.
- [72] T. E. Beechem, T. Ohta, B. Diaconescu, J. T. Robinson, *ACS Nano* **2014**, *8*, 1655.
- [73] A. Uri, S. Grover, Y. Cao, J. A. Crosse, K. Bagani, D. Rodan-Legrain, Y. Myasoedov, K. Watanabe, T. Taniguchi, P. Moon, M. Koshino, P. Jarillo-Herrero, E. Zeldov, *Nature* **2020**, *581*, 47.
- [74] C. Duan, Z. Cheng, B. Wang, J. Zeng, J. Xu, J. Li, W. Gao, K. Chen, *Small* **2021**, *17*, 2007306.
- [75] R. Xiong, J. Luan, S. Kang, C. Ye, S. Singamaneni, V. V. Tsukruk, *Chem. Soc. Rev.* **2020**, *49*, 983.
- [76] J. Lv, D. Ding, X. Yang, K. Hou, X. Miao, D. Wang, B. Kou, L. Huang, Z. Tang, *Angew. Chem., Int. Ed.* **2019**, *58*, 7783.
- [77] H. Hu, S. Sekar, W. Wu, Y. Battie, V. Lemaire, O. Arteaga, L. V. Poulikakos, D. J. Norris, H. Giessen, G. Decher, M. Pauly, *ACS Nano* **2021**, *15*, 13653.
- [78] R. Blell, X. Lin, T. Lindström, M. Ankerfors, M. Pauly, O. Felix, G. Decher, *ACS Nano* **2017**, *11*, 84.
- [79] H. Hu, M. Pauly, O. Felix, G. Decher, *Nanoscale* **2017**, *9*, 1307.
- [80] Y. Xia, Y. Yin, Y. Lu, J. McLellan, *Adv. Funct. Mater.* **2003**, *13*, 907.
- [81] C. Hanske, M. Tebbe, C. Kuttner, V. Bieber, V. V. Tsukruk, M. Chanana, T. A. F. König, A. Fery, *Nano Lett.* **2014**, *14*, 6863.
- [82] Z. Püspöki, M. Storath, D. Sage, M. Unser, *Adv. Anat., Embryol. Cell Biol.* **2016**, *219*, 69.
- [83] E. Fonck, G. G. Feigl, J. Fasel, D. Sage, M. Unser, D. A. Rüfenacht, N. Stergiopoulos, *Stroke* **2009**, *40*, 2552.
- [84] F. Kim, S. Kwan, J. Akana, P. Yang, *J. Am. Chem. Soc.* **2001**, *123*, 4360.
- [85] S. Shi, L. D. Sun, Y. X. Xue, H. Dong, K. Wu, S. C. Guo, B. T. Wu, C. H. Yan, *Nano Lett.* **2018**, *18*, 2964.
- [86] S. Kang, T. Kim, S. Cho, Y. Lee, A. Choe, B. Walker, S. J. Ko, J. Y. Kim, H. Ko, *Nano Lett.* **2015**, *15*, 7933.
- [87] Y. Huang, X. Duan, Q. Wei, C. M. Lieber, *Science* **2001**, *291*, 630.
- [88] J. Yao, H. Yan, C. M. Lieber, *Nat. Nanotechnol.* **2013**, *8*, 329.
- [89] C. W. Qiu, T. Zhang, G. Hu, Y. Kivshar, *Nano Lett.* **2021**, *21*, 5461.
- [90] N. I. Zheludev, Y. S. Kivshar, *Nat. Mater.* **2012**, *11*, 917.
- [91] J. B. Pendry, *Science* **2004**, *306*, 1353.
- [92] A. H. Dorrah, F. Capasso, *Science* **2022**, *376*, 367.
- [93] K. Konishi, M. Nomura, N. Kumagai, S. Iwamoto, Y. Arakawa, M. Kuwata-Gonokami, *Phys. Rev. Lett.* **2011**, *106*, 057402.
- [94] H. Liu, Z. Shang, X. Wu, C. Dou, J. Zhang, *Opt. Commun.* **2019**, *448*, 76.
- [95] M. Decker, M. W. Klein, M. Wegener, S. Linden, *Opt. Lett.* **2007**, *32*, 856.
- [96] Y. Liu, X. Zhang, *Chem. Soc. Rev.* **2011**, *40*, 2494.
- [97] A. Artar, A. A. Yanik, H. Altug, *Nano Lett.* **2011**, *11*, 1685.
- [98] E. Prodan, C. Radloff, N. J. Halas, P. Nordlander, *Science* **2003**, *302*, 419.
- [99] Z. Zhang, F. Fan, W. Shi, T. Zhang, S. Chang, *Biomed. Opt. Express* **2022**, *13*, 209.
- [100] F. Fang, Y. Cheng, H. Liao, *Optik* **2014**, *125*, 6067.
- [101] K. Tanaka, D. Arslan, S. Fasold, M. Steinert, J. Sautter, M. Falkner, T. Pertsch, M. Decker, I. Staude, *ACS Nano* **2020**, *14*, 15926.
- [102] H. X. Xu, G. Hu, L. Han, M. Jiang, Y. Huang, Y. Li, X. Yang, X. Ling, L. Chen, J. Zhao, C.-W. Qiu, *Adv. Opt. Mater.* **2019**, *7*, 1801479.

- [103] W. Ma, F. Cheng, Y. Liu, *ACS Nano* **2018**, *12*, 6326.
- [104] M. Decker, M. Ruther, C. E. Kriegler, J. Zhou, C. M. Soukoulis, S. Linden, M. Wegener, *Opt. Lett.* **2009**, *34*, 2501.
- [105] M. Kuwata-Gonokami, N. Saito, Y. Ino, M. Kauranen, K. Jefimovs, T. Vallius, J. Turunen, Y. Svirko, *Phys. Rev. Lett.* **2005**, *95*, 227401.
- [106] J. Rodríguez-Álvarez, A. García-Martín, A. Fraile Rodríguez, X. Batlle, A. Labarta, *Sci. Rep.* **2022**, *12*, 26.
- [107] B. Ai, H. M. Luong, Y. Zhao, *Nanoscale* **2020**, *12*, 2479.
- [108] X. R. Mao, Z. K. Shao, H. Y. Luan, S. L. Wang, R. M. Ma, *Nat. Nanotechnol.* **2021**, *16*, 1099.
- [109] J. Kim, D. Jeon, J. Seong, T. Badloe, N. Jeon, G. Kim, J. Kim, S. Baek, J. L. Lee, J. Rho, *ACS Nano* **2022**, *16*, 3546.
- [110] Y. Cui, L. Kang, S. Lan, S. Rodrigues, W. Cai, *Nano Lett.* **2014**, *14*, 1021.
- [111] N. Liu, H. Liu, S. Zhu, H. Giessen, *Nat. Photonics* **2009**, *3*, 157.
- [112] M. Cen, J. Wang, J. Liu, H. He, K. Li, W. Cai, T. Cao, Y. J. Liu, *Adv. Mater.* **2022**, *34*, 2203956.
- [113] V.-C. Su, C. H. Chu, G. Sun, D. P. Tsai, *Opt. Express* **2018**, *26*, 13148.
- [114] J. Chi, H. Liu, Z. Wang, N. Huang, *Opt. Express* **2020**, *28*, 4529.
- [115] J. Mun, M. Kim, Y. Yang, T. Badloe, J. Ni, Y. Chen, C. W. Qiu, J. Rho, *Light: Sci. Appl.* **2020**, *9*, 139.
- [116] N. Engheta, *IEEE Antennas Wireless Propag. Lett.* **2002**, *1*, 10.
- [117] V. V. Varadan, A. R. Tellakula, *J. Appl. Phys.* **2006**, *100*, 034910.
- [118] B. Wang, J. Zhou, T. Koschny, M. Kafesaki, C. M. Soukoulis, *J. Opt. A: Pure Appl. Opt.* **2009**, *11*, 114003.
- [119] R. Zhao, T. Koschny, C. M. Soukoulis, *Opt. Express* **2010**, *18*, 14553.
- [120] S. S. Oh, O. Hess, *Nano Convergence* **2015**, *2*, 24.
- [121] Y. Zhao, N. Engheta, A. Alù, *Metamaterials* **2011**, *5*, 90.
- [122] A. Alù, N. Engheta, *J. Opt. Soc. Am. B* **2006**, *23*, 571.
- [123] S. Bassiri, C. H. Papas, N. Engheta, *J. Opt. Soc. Am. A* **1988**, *5*, 1450.
- [124] Y. Cheng, F. Chen, H. Luo, *Phys. Lett., Sect. A: Gen. At. Solid State Phys.* **2020**, *384*, 126398.
- [125] L. Wu, Z. Yang, Y. Cheng, Z. Lu, P. Zhang, M. Zhao, R. Gong, X. Yuan, Y. Zheng, J. Duan, *Opt. Express* **2013**, *21*, 5239.
- [126] H. L. Liu, B. Zhang, T. Gao, X. Wu, F. Cui, W. Xu, *Nanoscale* **2019**, *11*, 5506.
- [127] Y. Tang, A. E. Cohen, *Phys. Rev. Lett.* **2010**, *104*, 163901.
- [128] E. Mohammadi, A. Tavakoli, P. Dehkoda, Y. Jahani, K. L. Tsakmakidis, A. Tittl, H. Altug, *ACS Photonics* **2019**, *6*, 1939.
- [129] T. Wu, S. Hou, W. Zhang, X. Zhang, *Phys. Rev. A* **2020**, *102*, 053519.
- [130] E. Hendry, T. Carpy, J. Johnston, M. Popland, R. V. Mikhaylovskiy, A. J. Laphorn, S. M. Kelly, L. D. Barron, N. Gadegaard, M. Kadodwala, *Nat. Nanotechnol.* **2010**, *5*, 783.
- [131] C. Kelly, R. Tullius, A. J. Laphorn, N. Gadegaard, G. Cooke, L. D. Barron, A. S. Karimullah, V. M. Rotello, M. Kadodwala, *J. Am. Chem. Soc.* **2018**, *140*, 8509.
- [132] A. Kuzyk, R. Schreiber, H. Zhang, A. O. Govorov, T. Liedl, N. Liu, *Nat. Mater.* **2014**, *13*, 862.
- [133] X. Lin, Z. Liu, T. Stauber, G. Gómez-santos, F. Gao, H. Chen, B. Zhang, T. Low, *Phys. Rev. Lett.* **2020**, *125*, 77401.
- [134] G. Li, A. Luican, J. M. B. Lopes Dos Santos, A. H. Castro Neto, A. Reina, J. Kong, E. Y. Andrei, *Nat. Phys.* **2010**, *6*, 109.
- [135] J. Henzie, M. H. Lee, T. W. Odom, *Nat. Nanotechnol.* **2007**, *2*, 549.
- [136] X. T. Kong, R. Zhao, Z. Wang, A. O. Govorov, *Nano Lett.* **2017**, *17*, 5099.
- [137] R. Knipper, T. G. Mayerhöfer, V. Kopecký, U. Huebner, J. Popp, *ACS Photonics* **2018**, *5*, 1176.
- [138] S. Takahashi, T. Tajiri, Y. Ota, J. Tatebayashi, S. Iwamoto, Y. Arakawa, *Appl. Phys. Lett.* **2014**, *105*, 051107.
- [139] Z. Wu, X. Chen, M. Wang, J. Dong, Y. Zheng, *ACS Nano* **2018**, *12*, 5030.
- [140] Y. Kim, B. Yeom, O. Arteaga, S. J. Yoo, S. G. Lee, J. G. Kim, N. A. Kotov, *Nat. Mater.* **2016**, *15*, 461.
- [141] G. Chu, X. Wang, T. Chen, J. Gao, F. Gai, Y. Wang, Y. Xu, *ACS Appl. Mater. Interfaces* **2015**, *7*, 11863.
- [142] X. Lan, X. Lu, C. Shen, Y. Ke, W. Ni, Q. Wang, *J. Am. Chem. Soc.* **2015**, *137*, 457.
- [143] K. Matsuo, K. Gekko, *Carbohydr. Res.* **2004**, *339*, 591.
- [144] M. Schulz, J. Zablocki, O. S. Abdullaeva, S. Brück, F. Balzer, A. Lützen, O. Arteaga, M. Schiek, *Nat. Commun.* **2018**, *9*, 2413.
- [145] M. V. Gorkunov, A. A. Antonov, Y. S. Kivshar, *Phys. Rev. Lett.* **2020**, *125*, 93903.
- [146] T. Shi, Z. L. Deng, G. Geng, X. Zeng, Y. Zeng, G. Hu, A. Overvig, J. Li, C. W. Qiu, A. Alù, Y. S. Kivshar, X. Li, *Nat. Commun.* **2022**, *13*, 4111.
- [147] A. Overvig, N. Yu, A. Alù, *Phys. Rev. Lett.* **2021**, *126*, 73001.
- [148] C. Bao, P. Tang, D. Sun, S. Zhou, *Nat. Rev. Phys.* **2022**, *4*, 33.
- [149] N. Amdursky, M. M. Stevens, *ChemPhysChem* **2015**, *16*, 2768.
- [150] E. Plum, J. Zhou, J. Dong, V. A. Fedotov, T. Koschny, C. M. Soukoulis, N. I. Zheludev, *Phys. Rev. B* **2009**, *79*, 035407.
- [151] M. Cheng, P. Fu, X. Tang, *Appl. Opt.* **2022**, *61*, 3054.
- [152] S. P. Rodrigues, S. Lan, L. Kang, Y. Cui, P. W. Panuski, S. Wang, A. M. Urbas, W. Cai, *Nat. Commun.* **2017**, *8*, 14602.
- [153] B. M. Maoz, A. Ben Moshe, D. Vestler, O. Bar-Elli, G. Markovich, *Nano Lett.* **2012**, *12*, 2357.
- [154] E. Plum, X. X. Liu, V. A. Fedotov, Y. Chen, D. P. Tsai, N. I. Zheludev, *Phys. Rev. Lett.* **2009**, *102*, 113902.
- [155] Z. Li, A. W. Clark, J. M. Cooper, *ACS Nano* **2016**, *10*, 492.
- [156] J. Fatome, S. Pitois, P. Morin, G. Millot, *Opt. Express* **2010**, *18*, 15311.
- [157] S. Wang, Z. L. Deng, Y. Wang, Q. Zhou, X. Wang, Y. Cao, B. O. Guan, S. Xiao, X. Li, *Light: Sci. Appl.* **2021**, *10*, 24.
- [158] L. Cong, P. Pitchappa, Y. Wu, L. Ke, C. Lee, N. Singh, H. Yang, R. Singh, *Adv. Opt. Mater.* **2017**, *5*, 1600716.
- [159] N. K. Grady, J. E. Heyes, D. R. Chowdhury, Y. Zeng, M. T. Reiten, A. K. Azad, A. J. Taylor, D. A. R. Dalvit, H. T. Chen, *Science* **2013**, *340*, 1304.
- [160] J.-G. Yun, S.-J. Kim, H. Yun, K. Lee, J. Sung, J. Kim, Y. Lee, B. Lee, *Opt. Express* **2017**, *25*, 14260.
- [161] P. C. K. Vesborg, T. F. Jaramillo, *RSC Adv.* **2012**, *2*, 7933.
- [162] Z. Wang, H. Jia, K. Yao, W. Cai, H. Chen, Y. Liu, *ACS Photonics* **2016**, *3*, 2096.
- [163] J.-H. Han, I. Kim, J.-W. Ryu, J. Kim, J.-H. Cho, G.-S. Yim, H.-S. Park, B. Min, M. Choi, *Opt. Express* **2015**, *23*, 17443.
- [164] I. Agranat, H. Caner, J. Caldwell, *Nat. Rev. Drug Discovery* **2002**, *1*, 753.
- [165] J. H. Kim, A. R. Scialli, *Toxicol. Sci.* **2011**, *122*, 1.
- [166] S. B. Tsogoeva, *N. Engl. J. Med.* **2021**, *385*, 2579.
- [167] Y. Qu, Y. Bai, T. Aba, H. Ullah, A. Abudukelimu, J. Huang, T. Gou, J. Li, Z. Zhang, *J. Phys. Chem. C* **2020**, *124*, 13912.
- [168] Y. Liu, Z. Wu, P. S. Kollipara, R. Montellano, K. Sharma, Y. Zheng, *ACS Nano* **2021**, *15*, 6448.
- [169] A. Rycerz, J. Tworzydło, C. W. J. Beenakker, *Nat. Phys.* **2007**, *3*, 172.
- [170] J. Isberg, M. Gabrysch, J. Hammersberg, S. Majdi, K. K. Kovi, D. J. Twitchen, *Nat. Mater.* **2013**, *12*, 760.
- [171] Z. Wu, J. Li, X. Zhang, J. M. Redwing, Y. Zheng, *Adv. Mater.* **2019**, *31*, 1904132.
- [172] Z. Li, C. Liu, X. Rong, Y. Luo, H. Cheng, L. Zheng, F. Lin, B. Shen, Y. Gong, S. Zhang, Z. Fang, *Adv. Mater.* **2018**, *30*, 1801908.
- [173] W. H. Lin, P. C. Wu, H. Akbari, G. R. Rossman, N. C. Yeh, H. A. Atwater, *Adv. Mater.* **2022**, *34*, 2104863.
- [174] J.-X. Li, W. Li, S. Hung, P. Chen, Y. Yang, T. Chang, P. Chiu, H. Jeng, C. Liu, *Nat. Nanotechnol.* **2022**, *17*, 721.
- [175] H. Zeng, J. Dai, W. Yao, D. Xiao, X. Cui, *Nat. Nanotechnol.* **2012**, *7*, 490.
- [176] M. Tamagnone, A. Ambrosio, K. Chaudhary, L. A. Jauregui, P. Kim, W. L. Wilson, F. Capasso, *Sci. Adv.* **2018**, *4*, eaat7189.
- [177] W. Ali, M. F. Mideksa, K. Hou, H. Li, X. Wang, Z. Tang, *Adv. Opt. Mater.* **2020**, *8*, 2000447.

- [178] A. G. Ricciardulli, S. Yang, J. H. Smet, M. Saliba, *Nat. Mater.* **2021**, 20, 1325.
- [179] M. Mayer, M. J. Schnepf, T. A. F. König, A. Fery, *Adv. Opt. Mater.* **2019**, 7, 1800564.
- [180] Z. Liu, D. Zhu, L. Raju, W. Cai, *Adv. Sci.* **2021**, 8, 2002923.
- [181] C. Zheng, G. Hu, X. Liu, X. Kong, L. Wang, C. W. Qiu, *ACS Nano* **2022**, 16, 13241.
- [182] A. Poddubny, I. Iorsh, P. Belov, Y. Kivshar, *Nat. Photonics* **2013**, 7, 948.
- [183] T. N. Ikeda, *Phys. Rev. Res.* **2020**, 2, 032015.
- [184] S. P. Rodrigues, S. Lan, L. Kang, Y. Cui, W. Cai, *Adv. Mater.* **2014**, 26, 6157.
- [185] M. J. Huttunen, G. Bautista, M. Decker, S. Linden, M. Wegener, M. Kauranen, *Opt. Mater. Express* **2011**, 1, 46.
- [186] L. Kang, C. Y. Wang, X. Guo, X. Ni, Z. Liu, D. H. Werner, *Nano Lett.* **2020**, 20, 2047.
- [187] V. K. Valev, J. J. Baumberg, B. De Clercq, N. Braz, X. Zheng, E. J. Osley, S. Vandendriessche, M. Hojeij, C. Blejean, J. Mertens, C. G. Biris, V. Volskiy, M. Ameloot, Y. Ekinici, G. A. E. Vandenbosch, P. A. Warburton, V. V. Moshchalkov, N. C. Panoiu, T. Verbiest, *Adv. Mater.* **2014**, 26, 4074.
- [188] M. He, J. Cai, Y.-H. Zhang, Y. Liu, Y. Li, T. Taniguchi, K. Watanabe, D. H. Cobden, M. Yankowitz, X. Xu, eprint,arXiv:2109.08255, **2021**.
- [189] Q. Li, B. Cheng, M. Chen, B. Xie, Y. Xie, P. Wang, F. Chen, Z. Liu, K. Watanabe, T. Taniguchi, S.-J. Liang, D. Wang, C. Wang, Q.-H. Wang, J. Liu, F. Miao, *Nature* **2022**, 609, 479.
- [190] Z. L. Deng, T. Shi, A. Krasnok, X. Li, A. Alù, *Nat. Commun.* **2022**, 13, 8.
- [191] H. Polshyn, M. Yankowitz, S. Chen, Y. Zhang, K. Watanabe, T. Taniguchi, C. R. Dean, A. F. Young, *Nat. Phys.* **2019**, 15, 1011.
- [192] S. Zhang, A. Song, L. Chen, C. Jiang, C. Chen, L. Gao, Y. Hou, L. Liu, T. Ma, H. Wang, X.-Q. Feng, Q. Li, *Sci. Adv.* **2020**, 6, eabc5555.
- [193] Y. Yu, K. Zhang, H. Parks, M. Babar, S. Carr, I. M. Craig, M. Van Winkle, A. Lyssenko, T. Taniguchi, K. Watanabe, V. Viswanathan, D. K. Bediako, *Nat. Chem.* **2022**, 14, 267.
- [194] Y. Zhang, F. Zhang, Z. Yan, Q. Ma, X. Li, Y. Huang, J. A. Rogers, *Nat. Rev. Mater.* **2017**, 2, 17019.
- [195] Z. Liu, H. Du, J. Li, L. Lu, Z. Y. Li, N. X. Fang, *Sci. Adv.* **2018**, 4, eaat4436.
- [196] L. Cong, P. Pitchappa, N. Wang, R. Singh, *Research* **2019**, 2019, 7084251.



Zexiang Han received his integrated M.Eng. degree in Materials Science and Engineering from Imperial College London, UK (2021). He is currently a research intern working under the supervision of Prof. Xiaoli Wang and Prof. Zhiyong Tang at the National Center for Nanoscience and Technology, China. His research interests include nanomaterials, chirality, self-assembly, and bio-nanointerfaces.



Xiaoli Wang received her Ph.D. degree from Université Pierre et Marie Curie-Paris VI in 2013. Afterward, she went to Chalmers University of Technology in Sweden to work as a postdoctoral fellow. Now Xiaoli Wang is an associate professor at the National Center for Nanoscience and Technology, China. Her current research interests are nanophotonics, plasmonics, ultrafast optics, and optical tweezers. She is especially focused on studies of plasmon-induced hot electron dynamics and applications now.



Zhiyong Tang obtained his Ph.D. degree from the Chinese Academy of Sciences in 2000 under the direction of Prof. Er kang Wang. After finishing his postdoctoral training at both Swiss Federal Institute of Technology Zurich and University of Michigan, he came back to China and took a professor position at National Center for Nanoscience and Technology at the end of 2006. His main research interests are focused on preparation, assembly, and application of functional nanomaterials.